

4-2012

Refinement of the Cast Microstructure of Hypereutectic Aluminum-Silicon Alloys with an Applied Electric Potential

Alexander Joseph Plotkowski
Grand Valley State University

Follow this and additional works at: <http://scholarworks.gvsu.edu/theses>

 Part of the [Engineering Commons](#)

Recommended Citation

Plotkowski, Alexander Joseph, "Refinement of the Cast Microstructure of Hypereutectic Aluminum-Silicon Alloys with an Applied Electric Potential" (2012). *Masters Theses*. 15.
<http://scholarworks.gvsu.edu/theses/15>

This Thesis is brought to you for free and open access by the Graduate Research and Creative Practice at ScholarWorks@GVSU. It has been accepted for inclusion in Masters Theses by an authorized administrator of ScholarWorks@GVSU. For more information, please contact scholarworks@gvsu.edu.

Refinement of the Cast Microstructure of Hypereutectic Aluminum-Silicon Alloys with
an Applied Electric Potential

Alexander Joseph Plotkowski

A Thesis Submitted to the Graduate Faculty of

GRAND VALLEY STATE UNIVERSITY

In

Partial Fulfillment of the Requirements

For the Degree of

Master of Science in Engineering

Padnos College of Engineering and Computing

April 2012

Acknowledgements

First, I would like to acknowledge my family and my fiancée, Andrea Mitchell, for their continual support throughout the arduous, but rewarding time spent preparing this thesis. I would particularly like to thank my advisor, Dr. Anyalebechi, who has been a mentor to me academically, professionally, and personally. Finally, I would like to thank Mr. Bob Bero, who made the experimentation so central to my research not only possible, but enjoyable.

Abstract

Hypereutectic aluminum-silicon (Al-Si) alloys are widely used in the aerospace and automobile industries because of their low density, excellent wear and corrosion resistance, low coefficient of thermal expansion, good strength, and excellent castability. They are used in applications that typically require a combination of light weight and high wear resistance, such as liner-less engine blocks, pistons, and pumps. However, the performance of these alloys depends on the fineness of their cast microstructure, especially dendrite cell size, primary and eutectic silicon particles. In this study, the effects of applied electric current on the cast microstructure of Al-13 wt.% Si and Al-20 wt.% Si were investigated. This involved application of a steady electric current density of about 500 mA/cm² during solidification of laboratory-size ingots in a metal mold. Microscopic examination of the cast ingots with a metallurgical microscope revealed that the applied electric refined the cast microstructure of the hypereutectic Al-Si alloys. Specifically, it appeared that the electric current changed the size distribution of the primary silicon particles by increasing the population of comparatively smaller size particles, although it did not affect the eutectic silicon particles. The applied electric current also decreased the average dendrite cell size. The extent of the observed cast microstructure refinement was less than the reported effects of applied electric current in the technical literature. It was also significantly less than the effects of traditional refinement obtained by addition of strontium and phosphorus to the molten hypereutectic Al-Si alloys prior to casting.

Table of Contents	Page No.
Abstract	iv
Table of Contents	v
List of Figures	vii
List of Tables	xi
Chapter 1 - Introduction	
1.1. Statement of Problem	1
1.2. Research Objectives	3
1.3. Technical Approach	4
1.4. References	6
Chapter 2 - Refinement of Cast Al-Si Microstructures	
2.1. Introduction	12
2.2. Chemical Modification of Cast Al-Si Microstructures	16
2.2.1. Chemical Modification of Eutectic Silicon Particles	16
2.2.2. Chemical Modification of Primary Silicon Particles	19
2.3. Physical Methods of Refinement of Cast Microstructure of Al-Si Alloys	22
2.4. Refinement of Cast Microstructure by an Applied Electric Current	26
2.4.1. High Electric Current Density Regime	27
2.4.2. Low Electric Current Density Regime	34
2.4. References	39
Chapter 3 - Experimental Work	
3.1. Introduction	50
3.2. Casting Process Selection and Mold Design	50
3.3. Rationale for Choice of Experimental Conditions	52
3.3.1. Alloy Composition	52
3.3.2. Casting Shape and Size	53
3.3.3. Thermocouple Design, Placement, and Data Collection	54
3.3.4. Electric Current Application	55
3.3.5. Casting Conditions	58
3.4. Preparation of Cast Ingots	59
3.5. Characterization of the Cast Ingot Microstructures	61
3.6. References	63
Chapter 4 - Results and Discussion	
4.1. Introduction	65
4.2. Local Solidification Rates	65
4.3. Cast Microstructures	67

4.4.	Effects of Applied Electric Current on Cast Microstructure	69
4.4.1.	Dendrite Cell Size	71
4.4.2.	Primary Silicon Particles	74
4.4.3.	Eutectic Silicon Particles	78
4.5.	Discussion	80
4.5.1.	Dendrite Cell Size	81
4.5.2.	Primary Silicon Particles	85
4.5.3.	Eutectic Silicon Particle	82
4.6.	References	89
Chapter 5 - Conclusions and Suggested Future Research		
5.1.	Conclusions	92
5.2.	Suggested Future Research	93

List of Figures	Page No.
Figure 2.1: Equilibrium phase diagram showing the binary Al-Si system.	13
Figure 2.2: Wear rate as a function of silicon content for various contact pressures.	14
Figure 2.3: Effect of chemical modification on the wear resistance of eutectic (LM-6) and near-eutectic (Al-21Si) alloys.	14
Figure 2.4: Comparison of (a) unmodified eutectic structure, (b) Sr modified eutectic structure, and (c) Sb modified eutectic structure.	17
Figure 2.5: Histogram showing refinement of primary silicon particles in Al-20 wt.% Si alloys using Al ₂ O ₃ nanoparticles.	21
Figure 2.6: Effect of Al ₂ O ₃ nanoparticles on mechanical properties of Al-20 wt.% Si alloys compared to ultrasonic and phosphorus modified conditions.	21
Figure 2.7: Schematic of mechanical mold vibration apparatus with an electrical resistance furnace.	23
Figure 2.8: SEM photomicrograph of A356 alloy solidified without (a) and with (b) ultrasonic vibration treatment.	23
Figure 2.9: Change in equivalent diameter of primary silicon particles in Al-18 wt.% Si alloy using electromagnetic vibration with different current densities and magnetic fluxes.	24
Figure 2.10: Schematic of intensive melt shearing apparatus.	26
Figure 2.11: Lamellar eutectic structure found after application of high density pulsed electric current to eutectic Al-Si alloy.	30
Figure 2.12: Optical photomicrographs of eutectic silicon particles in Al-6.6 wt.% Si alloys without electric current application (a), with direct current application (b), and with alternating current application (c).	31
Figure 2.13: Size of eutectic silicon particles in Al-17 wt.% Si with pulsed electric current application (a), and without current application (b).	32

Figure 2.14: SEM photomicrographs showing difference in size of primary silicon particles with applied electric current (a), and without applied electric current (b).	33
Figure 2.15: Primary silicon particles in Al-22 wt.% Si alloys without pulsed electric current at center of casting (a) and edge of casting (b), with 3 kV pulsed current application at center (c), and edge (d) of casting, and with 6 kV of pulsed current application at center (e) and edge of casting (f).	34
Figure 2.16: Polarized light photomicrographs showing the effect of applied electric current of varying types and current densities on the grain size of a 7050 aluminum alloy.	37
Figure 2.17: Average dendrite cell size as a function of solidification rate for a 7050 type aluminum alloy with and without electric current application.	38
Figure 2.18: Change in hardness of LM-25 Al-Si alloy as a function of current density applied in an alternating (a) and direct (b) manner.	38
Figure 3.1: Mold machined from mild steel. The two halves of the mold were located to each other using dowel pins.	51
Figure 3.2: The Al-Si phase diagram.	53
Figure 3.4: K type thermocouple with ceramic sleeve used for temperature measurement during solidification.	54
Figure 3.5.: Engineering drawing of mold showing thermocouple placement (dimensions in mm) and the corresponding data acquisition channel for each.	56
Figure 3.6: Schematic of electrode setup.	57
Figure 3.7: Photograph of the electrode setup at the mold prior to pouring.	57
Figure 3.8: Photograph of the power supply used to apply the electric current.	58
Figure 3.9: Mifco T-160 furnace and foundry equipment.	60
Figure 3.10: Schematic showing how each sample was cut around one of the thermocouples and the surface that was metallographically prepared.	62
Figure 3.11: Examples of cast ingots with thermocouples imbedded in castings.	62
Figure 3.12: Photograph of completed and assembled mold.	63
Figure 4.1: Comparison of cooling curves for Al - 13wt.% Si without and with electric current treatment as a function of distance from the top of the cast ingot.	66

Figure 4.2: Comparison of cooling curves for Al-20 wt.% Si without and with electric current treatment as a function of distance from the top of the cast ingot.	67
Figure 4.3: Solidification rates of each casting as a function of the distance from the top of the cast ingot.	69
Figure 4.4: Optical photomicrograph at 100x magnification of representative Al-13 wt.% Si cast microstructure, showing primary silicon particles, eutectic silicon particles, and eutectic aluminum dendrite cells.	70
Figure 4.5: Optical photomicrograph at 100x magnification of representative Al-20 wt.% Si cast microstructure, showing eutectic silicon particles, eutectic aluminum dendrite cells, and a large volume fraction of primary silicon particles.	70
Figure 4.6: Optical photomicrograph at 200x magnification showing an example of how each dendrite cell was measured at its widest point at locations where dendrites were clearly visible.	71
Figure 4.7: Average dendrite cell size as a function of alloy composition and application of electric current during solidification with respect to the local solidification time.	73
Figure 4.8: Average dendrite cell size as a function of alloy composition and application of electric current during solidification with respect to local solidification rate.	74
Figure 4.9: Optical photomicrographs at 200x magnification showing primary silicon particles in Al - 20wt.% Si without (a and c) and with (b and d) application of electric current during solidification.	75
Figure 4.10: Optical photomicrographs at 500x showing the difference in size of the smallest primary silicon particles in samples from the centers of Al - 20wt.% Si castings solidified (a) without electric current and (b) with electric current.	76
Figure 4.11: Very small primary silicon particles (200x magnification and 1000x magnification) in Al-20 wt.% Si with electric current applied during solidification.	76
Figure 4.12: Optical photomicrographs at 200x magnification of primary silicon particles in Al-13 wt.% Si alloy without (a and c) and with (b and d) application of electric current during solidification.	77
Figure 4.13: Optical photomicrographs at 500x magnification of primary silicon particles in Al-13 wt.% Si alloys cast without (a and c) and with (b and d) the application of electric current during solidification.	78

Figure 4.14: Optical photomicrographs at 100x magnification showing the large size distribution of eutectic silicon particles within a particular sample from Al - 13wt.% Si castings without current application (a and c) and with current application (b and d). 79

Figure 4.15: Optical photomicrographs at 500x showing no significant change in morphology of the eutectic silicon particles with the application of an electric current. Photomicrographs shown are from samples at the center of the castings. 80

Figure 4.16: Lamellar eutectic Si structure induced by the application of high density pulsed electric current during solidification of eutectic Al-Si alloy. 88

List of Tables	Page No.
Table 2.1: Comparison of mechanical properties of hypo and hypereutectic Al-Si alloys in as-cast conditions, and in hot extruded condition for hypereutectic composition.	15
Table 3.1: Experimental parameters of Al - 13wt.% Si castings with applied current.	60
Table 3.2: Experimental parameters for Al - 20 wt.% Si castings with applied current.	61
Table 4.1: Local solidification times and solidification rates for Al-13 wt.% Si castings.	68
Table 4.2: Average dendrite sizes and standard deviations for each composition and casting condition.	72
Table 4.3: Percent reduction in dendrite cell size as a result of the application of electric current during solidification as a function of distance from top of ingot for each alloy composition.	72
Table 4.4: Percent reduction in dendrite cell size with application of electric current for each alloy composition as a function of distance from top of ingot and p-values resulting from t-tests comparing the corresponding data sets.	82

Chapter 1

Introduction

1.1. Statement of Problem

Hypereutectic Al-Si alloys are widely used in the automobile and aerospace industries because they exhibit several specific and interesting properties, such as excellent wear resistance, high strength-to-weight ratio, low coefficient of thermal expansion, good corrosion resistance, excellent fluidity, and good castability [1-3]. They are used in various applications such as liner-less engine blocks [4], automotive pistons [5], compressor bodies, and pumps [6]. Hypereutectic Al-Si alloys are used to produce engine blocks without cylinder liners, automotive pistons, and a number of other products primarily because of their high wear resistance properties resulting from a large volume fraction of the silicon phase.

However, all of the aforementioned desirable properties of hypereutectic Al-Si alloys depend on the characteristics of their cast microstructures, namely secondary dendrite cell size or arm spacing, and the size, morphology (or shape), and distribution of eutectic and primary Si particles. The morphology of primary silicon particles can be rather complex, such as plate-like [7], star-shaped [7,8], polygonal, blocky, and feathery [9] varying with solidification conditions, chemical composition, and alloying elements.

Chapter 1 - Introduction

In these forms, primary silicon particles compromise the machinability, wear resistance, and mechanical properties of the alloy castings. Refinement and control of the eutectic and primary silicon particles is an effective way of improving the properties of the hypereutectic Al-Si alloys. For examples, hypereutectic Al-Si alloys with a uniform distribution of fine primary silicon particles have higher strength and better wear resistance.

Several different techniques have been proposed for the refinement of eutectic and primary silicon particles in hypereutectic Al-Si alloys. They include: (i) chemical treatments by addition of elements such as Na, P, Sr, La, etc. [3,10,11], (ii) mechanical stirring [12], (iii) electromagnetic stirring [9,13,14] and vibration [15], (iv) ultrasonic treatment [16], and (v) application of an electric current during solidification [5,17].

The purpose of this study is to investigate the effect of an applied electric current on the microstructure of hypereutectic Al-Si alloys. The motivation for this research is based in an industrial interest in the refinement and modification of these alloys and a dissatisfaction with current refinement methods that stem from a variety of technological, practical, and environmental issues [11,18]. As such, an effective solution that is easily implemented and avoids the drawbacks of the traditional techniques would be readily adopted by the aluminum industry. One potential alternative to the tradition refinement techniques is the application of an electric current to the casting during solidification, and previous research has shown that this process can produce significant refinement in a variety of cast materials [19–22]. However, few studies has been published on the application of this technique to Al-Si alloys [5,23,24]. This study experimentally assessed the effects of this technique on the microstructures of hypereutectic Al-Si alloys using

relatively low current densities and to compared these results with traditional methods of refinement.

1.2. Research Objectives

This study has been performed to determine the effects on cast microstructure, if any, of the application of electric current during solidification of hypereutectic Al-Si alloys. In order to accomplish this, the following major objectives were identified:

- (a) Design and assemble a casting apparatus that would allow the effective application of electric current to a solidifying molten material and the simultaneous measurement of the applied electric current and the rate of solidification of the solidifying casting.
- (b) Quantitatively determine the effect of an applied current on the characteristics of the microstructure of hypereutectic Al-Si alloys, namely: (i) secondary dendrite cell size or arm spacing, (ii) eutectic Si particle size and size distribution, and (iii) the primary Si particle size and size distribution.
- (c) Determine the effects of electric current density on the refinement, if any, of the hypereutectic Al-Si alloys.

- (d) Determine the effects of the chemical composition, specifically, the Si content, on the effects of electric current on the cast microstructure of hypereutectic Al-Si alloys.

- (e) Quantitatively determine the combined effects of solidification rate and electric current density on the cast microstructure of Al-Si alloys.

The focus of this study was on the application of direct electric current (DC) during solidification of Al-13 wt. Si and Al-20 wt.% Si hypereutectic alloys in a laboratory-size permanent mold.

1.3. Technical Approach

Hypereutectic Al-Si alloys are of technological interest because of the advantageous properties imparted to them by the high volume fraction of hard eutectic and primary silicon particles. Unfortunately, the morphology of the eutectic silicon particles is generally needle or plate-like and the primary silicon particles are large and faceted, producing stress concentrations that degrade the mechanical properties of the material. Therefore, it is often necessary to refine the size of these particles and to modify their morphologies.

Refinement and modification can be accomplished with increased cooling rates, but this approach is difficult to control and not practical for some casting processes or

castings with thin sections. Therefore, chemical modification is often used. It is well established that sodium or strontium can be used to refine the eutectic silicon from a plate like to a fibrous morphology, and that phosphorus can be used to refine the size and improve the morphology of the primary silicon particles. However, combining these elements to refine both structures in hypereutectic alloys is much less effective on both types of silicon particles than either element being used in isolation. Additionally, there are practical and environmental concerns associated with this method. Physical methods for refinement have been designed as an alternative to chemical modification. These include mechanical and electromagnetic vibration, mechanical and electromagnetic stirring, semi-solid processing, and intensive melt shearing. However, the equipment for these processes is generally complex and expensive, and these methods have yet to be widely implemented by the casting industry.

An additional technique for refinement is the application of an electric current to the casting during solidification. Previous studies have shown that this process is effective for a variety of metals, including cast iron [19,25], pure aluminum [22], and Al 7050 alloy [21], but few studies have been performed using this technique on Al-Si alloys [23,24], and fewer yet on hypereutectic Al-Si alloys [5]. Furthermore, these studies were conducted at relatively high current densities, but low current densities have been shown effective in other alloy systems [21,25,26]. Because of the widespread use of this group of alloys, it is of interest to further study the effectiveness of refinement using this method, and with the goal of minimizing power consumption, it is of particular interest to assess the effect at low current densities.

The current study performed castings of Al-13 wt.% Si and Al-20 wt.% Si alloys with and without the application of an electric current. The Al-13 wt.% Si castings are near the eutectic composition of the Al-Si system (12.6 wt.% Si) and were used to investigate the effects of the applied current on the eutectic silicon particles. The Al-20 wt.% Si castings were used to assess the effect of the current application on the primary silicon particles. The casting procedure was performed using a permanent mold machine from mild steel and the alloys of interest were melted using a natural gas furnace and poured manually. The electric current was supplied in a steady manner using a power supply with a current density of approximately $500\text{mA}/\text{cm}^2$. Temperature data was recorded using type K thermocouples at three location in each casting. The temperature data was used to compute local solidification times and rates, and these values were compared for each condition. Samples around each thermocouple were sectioned from the castings and metallographically prepared. Optical photomicrographs were taken of each sample in order to qualitatively assess the effect of the application of the electric current on the eutectic and primary silicon particles for each casting location. Additionally, dendrite cell sizes were quantitatively measured and compared as a function of current application and solidification rate.

1.5. References

- [1] B. K. Prasad, K. Venkateswarlu, O. P. Modi, A. K. Jha, S. Das, and R. Dasgupta, "Sliding Wear Behavior of Some Al-Si Alloys : Role of Shape and Size of Si

Chapter 1 - Introduction

- Particles and Test Conditions,” *Metallurgical and Materials Transactions A*, Nov. 1998, vol. 29, pp. 2747-2752.
- [2] D. K. Dwivedi, “Wear behaviour of cast hypereutectic aluminum silicon alloys,” *Materials & Design*, Jan. 2006, vol. 27, no. 7, pp. 610-616.
- [3] S. Hegde and K. N. Prabhu, “Modification of eutectic silicon in Al–Si alloys,” *Journal of Materials Science*, Mar. 2008, vol. 43, no. 9, pp. 3009-3027.
- [4] J. Jorstad, “The hypereutectic aluminum-silicon alloy used to cast the Vega engine block,” *Modern Casting*, 1971, vol. 60, no. 4, pp. 59-64.
- [5] D. Hongsheng, Z. Yong, J. Sanyong, C. Ruirun, and Z. Zhilong, “Influences of pulse electric current treatment on solidification microstructures and mechanical properties of Al-Si piston alloys,” *China Foundry*, 2008, vol. 6, no. 1, pp. 24-31.
- [6] J.-wei Yeh, S.-ying Yuan, and C.-hung Peng, “A reciprocating extrusion process for producing hypereutectic Al – 20wt. % Si wrought alloys,” *Materials Science and Engineering A*, 1998, vol. 252, pp. 212-221.
- [7] J. Y. Chang, G. H. Kim, I. G. Moon, and C. S. Choi, “Rare Earth Concentration in the Primary Si Crystal in Rare Earth Added Al-21wt.%Si Alloy,” *Acta Metallurgica*, 1998, vol. 39, no. 3, pp. 307-314.

Chapter 1 - Introduction

- [8] Q. C. Jiang, C. L. Xu, M. Lu, and H. Y. Wang, "Effect of new Al–P–Ti–TiC–Y modifier on primary silicon in hypereutectic Al–Si alloys," *Materials Letters*, Mar. 2005, vol. 59, no. 6, pp. 624-628.
- [9] F. C. Robles Hernández and J. H. Sokolowski, "Comparison among chemical and electromagnetic stirring and vibration melt treatments for Al–Si hypereutectic alloys," *Journal of Alloys and Compounds*, Dec. 2006, vol. 426, no. 1–2, pp. 205-212.
- [10] H. S. Dai and X. F. Liu, "Optimal holding temperatures and phosphorus additions for primary silicon refinement in Al–high Si alloys," *Materials Science and Technology*, Oct. 2009, vol. 25, no. 10, pp. 1183-1188.
- [11] D. P. Kanicki, "Processing molten aluminum - part 1 : understanding silicon modification," *Modern Casting*, Jan. 1990, pp. 24.
- [12] K. Sukumaran, B. . Pai, and M. Chakraborty, "The effect of isothermal mechanical stirring on an Al–Si alloy in the semisolid condition," *Materials Science and Engineering: A*, Mar. 2004, vol. 369, no. 1–2, pp. 275-283.
- [13] D. Lu, Y. Jiang, G. Guan, R. Zhou, Z. Li, and R. Zhou, "Refinement of primary Si in hypereutectic Al–Si alloy by electromagnetic stirring," *Journal of Materials Processing Technology*, Jul. 2007, vol. 189, no. 1–3, pp. 13-18.

Chapter 1 - Introduction

- [14] B. I. Jung, C. H. Jung, T. K. Han, and Y. H. Kim, "Electromagnetic stirring and Sr modification in A356 alloy," *Journal of Materials Processing Technology*, 2001, vol. 111, pp. 69-73.
- [15] J. Yu, Z. Ren, and K. Deng, "Refinement and migrating behaviors in Al-Si hypereutectic alloys solidified under electromagnetic vibration," *Acta Metallurgica Sinica*, 2011, vol. 24, no. 4, pp. 301-308.
- [16] X. Jian, T. T. Meek, and Q. Han, "Refinement of eutectic silicon phase of aluminum A356 alloy using high-intensity ultrasonic vibration," *Scripta Materialia*, Mar. 2006, vol. 54, no. 5, pp. 893-896.
- [17] C. Ban, Y. Han, Q. Ba, and J. Cui, "Influence of Pulse Electric Current on Solidification Structures of Al-Si Alloys," *Materials Science Forum*, 2007, vol. 546-549, pp. 723-728.
- [18] N. Abu-Dheir, M. Khraisheh, K. Saito, and A. Male, "Silicon morphology modification in the eutectic Al-Si alloy using mechanical mold vibration," *Materials Science and Engineering: A*, Feb. 2005, vol. 393, no. 1-2, pp. 109-117.
- [19] A. Misra, "Misra Technique Applied to Solidification of Cast Iron," *Metallurgical Transactions A*, Feb. 1986, vol. 16, pp. 358-360.

Chapter 1 - Introduction

- [20] J. Barnak and A. Sprecher, "Colony (grain) size reduction in eutectic Pb-Sn castings by electroplusing," *Scripta metallurgica et materialia*, 1995, vol. 32, no. 6, pp. 879-884.
- [21] P. N. Anyalebechi and K. M. Tomaswick, "Effect of Application of Electric Current During Solidification on the Cast Microstructure of Aluminum Alloy 7050," in *EPD Congress 2009*, 2009, pp. 541-554.
- [22] X. Liao, Q. Zhai, J. Luo, W. Chen, and Y. Gong, "Refining mechanism of the electric current pulse on the solidification structure of pure aluminum," *Acta Materialia*, May 2007, vol. 55, no. 9, pp. 3103-3109.
- [23] G. Xu, J. Zheng, Y. Liu, and J. Cui, "Effect of electric current on the cast microstructure of Al-Si alloy," *China Foundry*, 2005, vol. 2, no. 3, pp. 171-175.
- [24] Y. Zhang et al., "Influence of Electric-Current Pulse Treatment on the Formation of Regular Eutectic Morphology in an Al-Si Eutectic Alloy," *Metallurgical and Materials Transactions B*, Mar. 2011, vol. 42, no. 3, pp. 604-611.
- [25] K. Vashchenko, D. Chernega, S. Vorob'ev, N. Lysenko, and Y. Yakovchuk, "Effect of Electric Current on the Solidification of Cast Iron," *Metallovedenie i Termicheskaya Obrabotka Metallov*, Mar. 1974, vol. 3, pp. 62-65.

Chapter 1 - Introduction

- [26] A. K. Misra, "A Novel Solidification Technique of Metals and Alloys : Under the Influence of Applied Potential," *Metallurgical Transactions A*, Jul. 1985, vol. 24, pp. 1354-1355.

Chapter 2

Refinement of Cast Al-Si Microstructures

2.1. Introduction

Aluminum casting alloys are generally of interest because of their high specific strengths compared to other casting alloys such as cast irons or steels [1]. Furthermore, aluminum casting alloys have good castability, good fluidity, and comparably low melting points. Of the various elements commonly alloyed with aluminum for casting purposes, silicon is among the most popular, and Al-Si alloys constitute approximately 80% of the aluminum casting alloys [1]. This popularity is explained by the strength-to-weight ratio, superior fluidity, excellent wear and corrosion resistance, and low shrinkage and coefficient of thermal expansion of Al-Si alloys. Aluminum and silicon form a simple binary system with a eutectic at 12.6 wt.% Si and a temperature of 577 °C. Figure 2.1 shows the Al-Si equilibrium phase diagram.

Excellent wear resistance is commonly cited as one of the main motivating factors for the selection of hypereutectic Al-Si alloys for many applications, and automotive pistons in particular. However, wear is a complex phenomenon dependent on service conditions including load, speed, temperature, environment, and counterbody material [2], and wear resistance in Al-Si alloys as a function of silicon content is not well established. Clegg and Das found that wear resistance is highest for the eutectic composition, as shown in Figure 2.2 [3], but Wang et al. found that hypereutectic Al-Si alloys performed better than the eutectic alloy under high normal loads [4]. Additionally,

it has been found that the refinement of both the eutectic and primary silicon particles strongly influences the wear resistance [2,5,6]. Figure 2.3 shows an example of the improvement of wear resistance with microstructural refinement for eutectic and near eutectic Al-Si alloys [5].

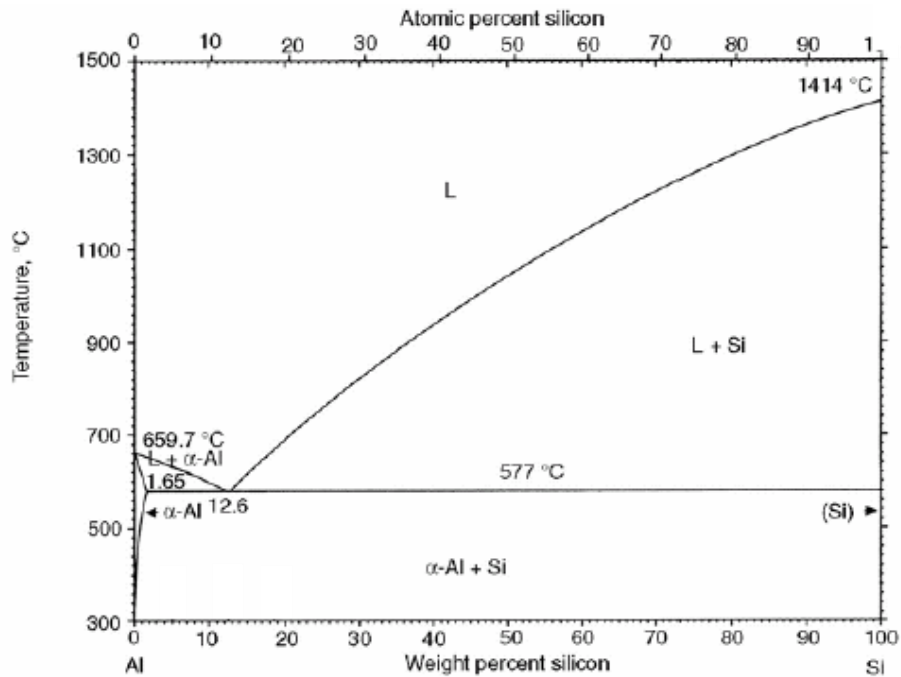


Figure 2.1: Equilibrium phase diagram showing the binary Al-Si system.

Physical and mechanical properties, such as density, yields strength, ultimate tensile strength, ductility, and hardness, are also influenced by silicon content in Al-Si alloys [2,7-9]. In hypoeutectic alloys, increased silicon content generally benefits these properties [7]. However, in hypereutectic alloys, coarse, faceted primary silicon particles produce stress concentrations that are detrimental to the mechanical properties of the material [10]. Table 2.1 shows a comparison of several mechanical properties for hypoeutectic and hypereutectic Al-Si alloys [7]. The ultimate tensile strength and ductility decreased for the hypereutectic case, but hot extruding the hypereutectic alloy

increased these properties to levels superior to that of the hypoeutectic alloys, as shown in the last row of Table 2.1, by reducing the size and increasing the uniformity of the primary silicon particles [7].

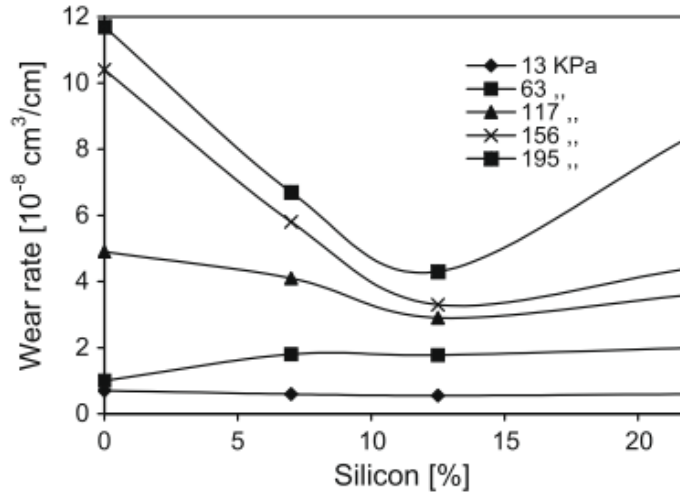


Figure 2.2: Wear rate as a function of silicon content for various contact pressures [3].

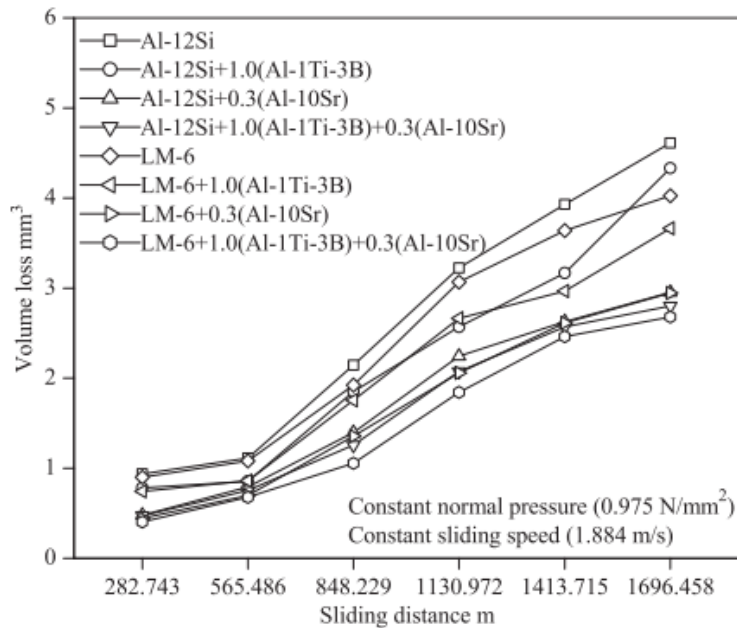


Figure 2.3: Effect of chemical modification on the wear resistance of eutectic (LM-6) and near-eutectic (Al-12Si) alloys [5].

Table 2.1.: Comparison of mechanical properties of hypo and hypereutectic Al-Si alloys in as-cast conditions, and in hot extruded condition for hypereutectic composition [7].

Material	0.2% YS (MPa)	UTS (MPa)	Ductility (%)	Microhardness (HV)
Al-7Si	55.3±2.1	141.7±2.1	12.2±0.5	38.5±1.2
Al-10Si	75.4±1.6	154.7±3.4	10.3±0.8	39.2±0.4
Al-19Si	80.8±3.2	129.6±8.7	2.3±1.9	43.4±2.1
Al-19Si(Ext)	82.7±3.1	189.0±12.1	21.4±8.8	59.2±0.5

Mechanical properties of Al-Si alloys can also be improved through the refinement of the eutectic silicon particles. These particles form with large plate or needle-like morphology under normal conditions [1], but can be modified to a fine fibrous structure that greatly improves the mechanical properties of the material [11-16]. As such, for hypereutectic Al-Si alloys, it is often of interest to refine both the eutectic and primary silicon phases to gain the best possible combination of properties.

To increase the mechanical properties of these alloys, it is therefore necessary to modify the size and morphology of both the eutectic and primary silicon particles. This refinement can be achieved using increased solidification rates, but this process is difficult to control and not applicable to all casting processes or castings with thin sections [13]. As such, chemical modification using sodium, phosphorus, or rare-earth metals has been widely used as a method for modification [1,17-19]. Alternatively, physical means of modification include semisolid processing, mechanical or electromagnetic stirring [15,20–22], mechanical and electromagnetic vibration [13,21,23,24], ultrasonic vibration [14], and intensive melt shearing [25,26].

One alternative to the traditional methods of refinement and modification is the application of an electric current to the melt during solidification. This process has proven effective in a variety of different alloy systems, including Al-Si alloys. The following presents an overview of modification techniques for both eutectic and primary silicon particles in Al-Si cast microstructures.

2.2. Chemical Modification of Cast Al-Si Microstructures

In hypereutectic Al-Si alloys, it is of interest to modify or refine both the eutectic and primary silicon particles. Chemical modification is a common route to achieving significant improvement in the size and morphology of both eutectic and primary silicon particles. However, the same chemical modifiers are not commonly used for both purposes. Simultaneous modification of both the eutectic and primary silicon particles in hypereutectic alloys is particularly difficult. Additionally, while a number of theories for the mechanisms of refinement exist, no theory fully explains the phenomenon, and it is still not well understood.

2.2.1. Chemical Modification of Eutectic Silicon Particles

Chemical modification of Al-Si alloys using certain elements can change the morphology of the eutectic silicon particles from a flake or needle-like to a fibrous

structure. The elements most commonly used are sodium and strontium, which alter the structure from flake-like to fibrous, and antimony, which refines the flake-like structure [12,27]. Figure 2.4 shows a comparison of modified and unmodified eutectic silicon structures comparing strontium and antimony modification [12]. Additionally, a variety of rare earth metals (Ba, Ca, Y, Yb) have been reported to have a similar effect on the eutectic structure [11]. While eutectic refinement is of considerable interest the mechanism of refinement is still not well understood [1,12]. Several mechanism theories have been proposed. The two main theories, being restricted growth and restricted nucleation, are briefly discussed here.

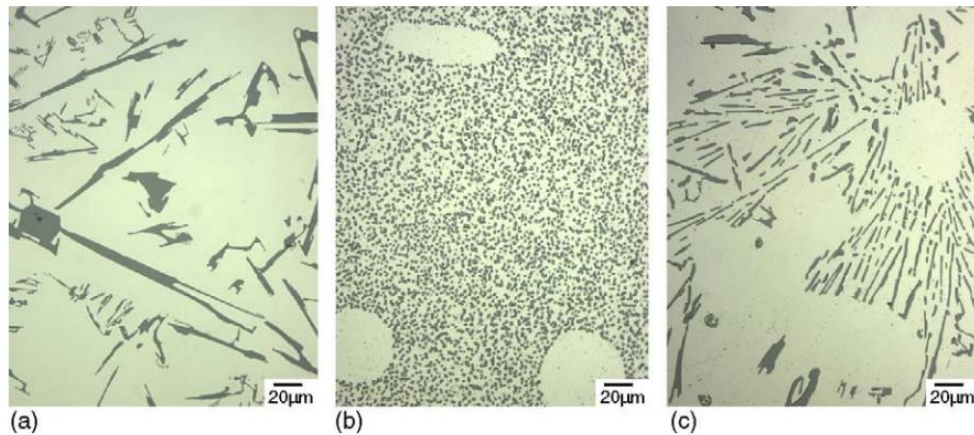


Figure 2.4: Comparison of (a) unmodified eutectic structure, (b) Sr modified eutectic structure, and (c) Sb modified eutectic structure [12].

One theory for the mechanism of chemical modification of the eutectic silicon particles, is that the atoms of the modifying element are absorbed into the growth steps of the silicon solid-liquid interface, causing a dramatic increase in twinning density, and thereby modifying the structure by inhibiting further growth of the silicon particle [28]. As such, this theory is generally referred to as the restricted growth theory [1]. This

theory is supported by the fact that modified eutectic particles contain significantly more twins than do particles in unmodified castings. In particular, it has been calculated that a growth twin is formed at the solid-liquid interface most readily if the ratio of the atomic radius of the modifying element to that of silicon (r/r_{si}) exceeds 1.65. However, several contradictions with this theory have been found [28]:

- i. While eutectic silicon particles in fibrous structures formed by modification contain a high density of twins, eutectic silicon particles in otherwise identical structures formed by quenching are relatively free of twins. The restricted growth theory does not explain the role of cooling rate in conjunction with impurity elements.
- ii. Even though sodium has a less than ideal atomic radius ($r/r_{si} = 1.59$) than calcium ($r/r_{si} = 1.68$) or ytterbium ($r/r_{si} = 1.66$), it is a superior modifier.
- iii. The restricted growth theory does not explain the well established phenomenon of over modification.

The second proposed mechanism is the restricted nucleation theory, in which the modifying element neutralizes the heterogeneous nucleation of silicon particles on AIP particles or reduces the diffusion coefficient of the silicon in the melt [1]. AIP particles are of interest because of their crystallographic similarity to silicon is sufficient to promote epitaxial growth, and greatly reduces the free energy barrier to nucleation [29].

By neutralizing the effect of these particles, undercooling of the melt before eutectic solidification is increased, and the resulting nucleation rate of eutectic silicon particles is increased, causing the observed modification [1]. Similarly, it has also been proposed that modifying elements halt the high temperature nucleation of iron containing phases. Silicon particles have a propensity to heterogeneously nucleate upon these phases at temperatures higher than the eutectic temperatures. These silicon particles then experience uninterrupted growth into the eutectic liquid in the unmodified plate-like form. Thus, by limiting the solidification of these iron containing phases, the growth of the eutectic silicon particles is impeded by solidified eutectic aluminum [30].

2.2.2. Chemical Modification of Primary Silicon Particles

In contrast to chemical modification of eutectic silicon particles, the mechanism for chemical modification of primary silicon particles is relatively well understood. It is generally agreed that modifying elements form compounds with aluminum that promote heterogeneous nucleation of silicon particles [10,12,18,31]. Thus, the quantity of primary silicon nuclei is dramatically increased, and given a finite amount of solute in the system, the average size of these particles decreases. The most common element used for primary silicon modification is phosphorus. It combines with aluminum to form AlP which is crystallographically similar to silicon and promotes epitaxial growth [10,29]. Additions of boron have also been shown to promote modification and increase the modification efficiency of phosphorus [31].

The problem of modifying both the eutectic and primary silicon particles in hypereutectic alloys is more difficult. While phosphorus effectively refines the primary particles, it does not refine or modify the eutectic particles. Furthermore, additions of both phosphorus and sodium, to refine primary and modify eutectic particles, respectively, are both much less effective than when added in isolation. This is presumably because they can react to form Na_3P [19]. Rare earth metals have been found to refine the primary silicon particles [11,17,18,32]. This is of particular interest since these elements can simultaneously be used to modify the eutectic structure, though not as efficiently as the traditionally used sodium [17]. Chong *et al.* found that additions of phosphorus could be used simultaneously with rare earth metals additions to significantly refine both the primary and the eutectic silicon phases [18].

Cicco *et al.* [33] showed that the addition of various nanoscale inoculants to molten A356 lowered the free energy barrier to nucleation. This resulted in a smaller amount of undercooling required to nucleate the primary Al phase. They found that the reduction of undercooling was a function of the crystal structure of the nanoparticle, i.e. $\gamma\text{-Al}_2\text{O}_3$ is a much more effective nucleation catalyst than $\alpha\text{-Al}_2\text{O}_3$. This result is consistent with the lattice disregistry theory for predicting the effectiveness of a nucleation catalyst within the adsorption and free growth model for heterogeneous nucleation. They postulated that this catalysis of nucleation would lead to the adoption of nanoparticles as microstructural refiners and could greatly improve the mechanical properties of cast materials.

Choi *et al.* demonstrated that modification of both the eutectic and primary silicon particles in hypereutectic Al-Si alloys can be achieved with the addition of $\gamma\text{-Al}_2\text{O}_3$

nanoparticles [34]. Figure 2.5 shows histograms of primary silicon particles size in Al-20 wt.% Si alloys treated with various amounts of Al₂O₃ nanoparticles additions.

Furthermore, it was also found that these nanoparticles reinforced the metal matrix, leading to higher ductility, yield strength, and ultimate tensile strength, than is found using traditional refinement techniques. These results are demonstrated in Figure 2.6 as compared to ultrasonic treated, phosphorus modified, and unmodified Al-20 wt.% Si.

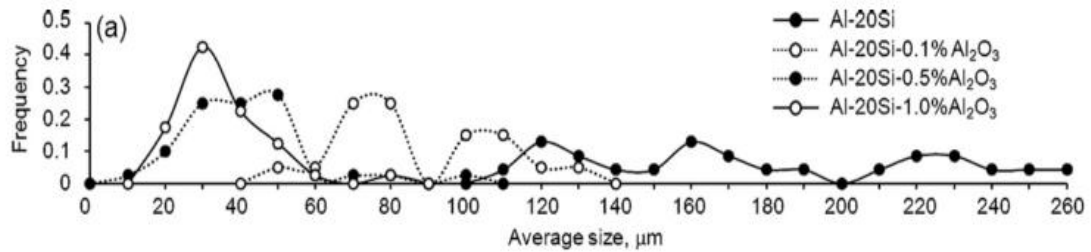


Figure 2.5: Histogram showing refinement of primary silicon particles in Al-20 wt.% Si alloys using Al₂O₃ nanoparticles [34].

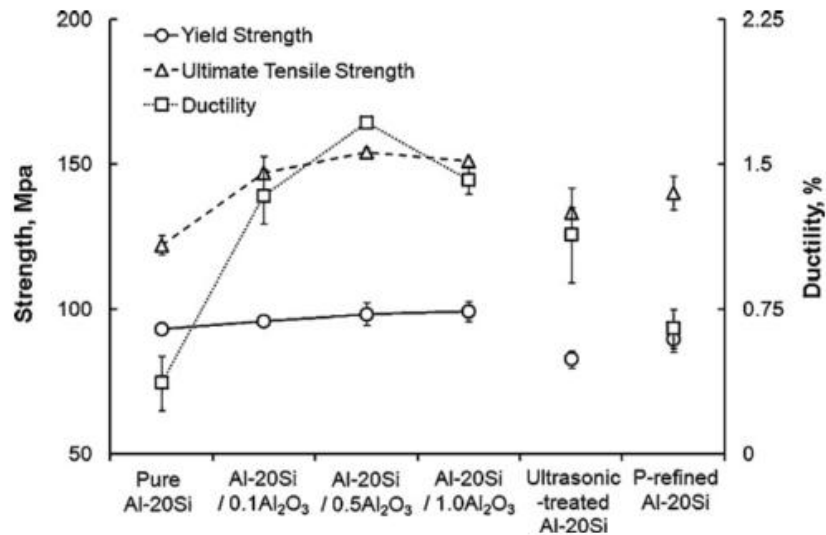


Figure 2.6: Effect of Al₂O₃ nanoparticles on mechanical properties of Al-20 wt.% Si alloys compared to ultrasonic and phosphorus modified conditions [34].

2.3. Physical Methods of Refinement of the Cast Microstructure of Al-Si Alloys

It is well known that increased solidification rate generally leads to the refinement of cast microstructures. In the case of Al-Si alloys, rapid solidification refines both the primary [35] and eutectic [11] silicon particles and also decreases the secondary dendrite arm spacing [35]. Unfortunately, in many industrial applications, achieving the desired solidification rate is neither physically, nor economically practical. A number of other methods for physically refining the microstructure of Al-Si alloys have been developed.

One method for physical refinement is mechanical vibration. In this method, the mold is subjected to a mechanical vibration with a particular frequency and amplitude. This vibration causes shearing of the dendrite arms, which float into the melt and promote increased nucleation. Figure 2.7 shows an example of an apparatus used to apply mechanical vibration to an aluminum melt during solidification. Taghavi et al. [36] found that mechanical vibration effectively refined the dendritic structure of A356 aluminum alloy, and that the level of refinement was directly related to the vibration frequency and the duration of the vibration treatment. Abu-Dheir et al. [13] reported that the application of this method to eutectic Al-Si alloys refined the eutectic and the dendritic structure of as-cast samples, although the refinement was not as significant as that observed with chemical modification. Additionally, it was found that the refinement was a strong function of the vibration amplitude, with a characteristic value that yielded maximum refinement, beyond which coarsening was observed.

Similar to mechanical vibration, ultrasonic vibrations can also be applied during solidification to refine microstructures. Using high intensity ultrasonic vibrations, Jian et

al. [14] observed significant refinement of both the eutectic silicon particles and α -Al dendrites in A356 alloys. Figure 2.8 shows scanning electron photomicrographs of A356 alloy solidified with and without ultrasonic vibration. While these mechanical vibration methods are effective, they face challenges for application to large permanent and sand molds, and because of the high cost of the equipment involved.

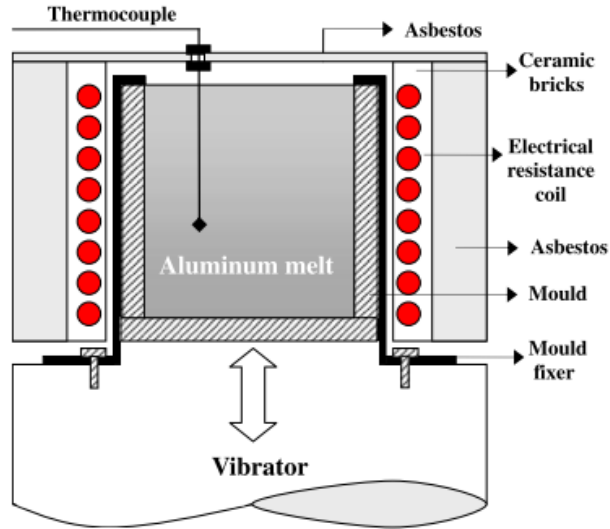


Figure 2.7: Schematic of mechanical mold vibration apparatus with an electrical resistance furnace [36].

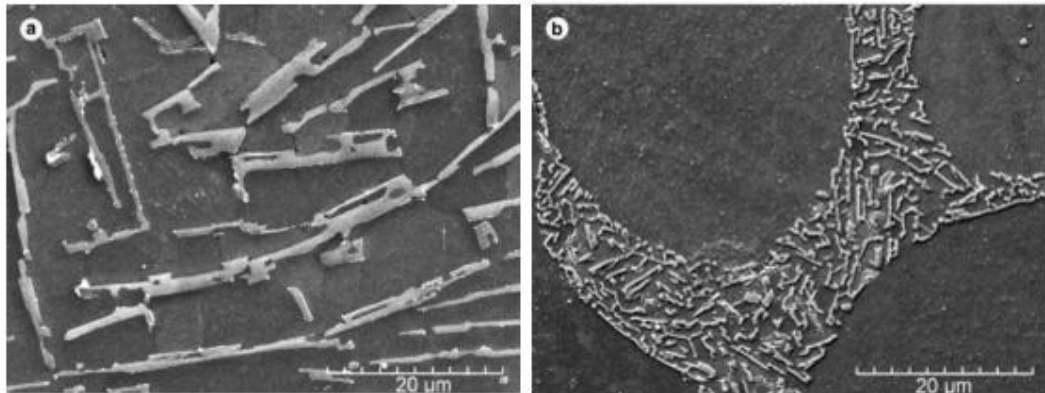


Figure 2.8: SEM photomicrographs of A356 alloy solidified without (a) and with (b) ultrasonic vibration treatment [14].

Similar to mechanical vibration, electromagnetic vibration has been used as a method for microstructural refinement that does not involve contacting the mold. Instead, the vibration is induced by applying orthogonal static magnetic and alternating electric fields [13]. Radjai et al. [24] studied the effect of such a vibration on the refinement of Al - 17 wt.% Si and concluded that electromagnetic vibration caused a cavitation effect that crushed the primary silicon particles into smaller pieces. Similarly, Yu et al. [23] found significant refinement of the primary silicon particles with the application of this technique. Figure 2.9 shows the change in equivalent diameter of the primary silicon particles as a function of current density and magnetic flux used to create the electromagnetic vibrations. Unfortunately, electromagnetic vibration faces many of the same problems for implementation as mechanical vibration in that it is not well suited for large molds or sand casting, and that the equipment is expensive [13].

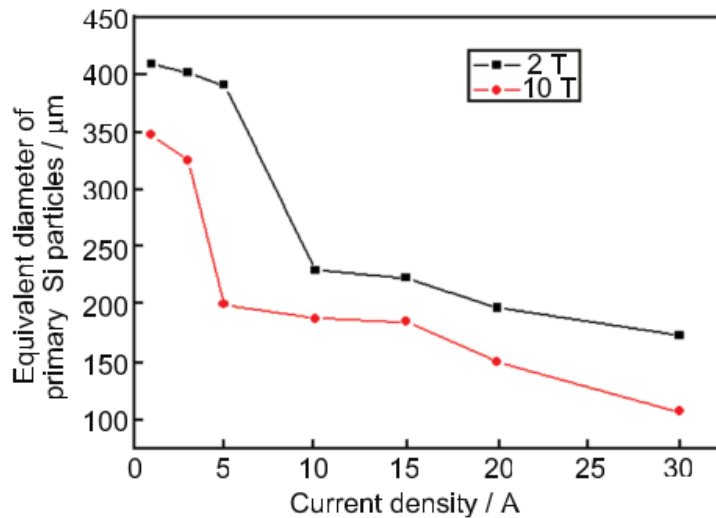


Figure 2.9: Change in equivalent diameter of primary silicon particles in Al-18 wt.% Si alloy using electromagnetic vibration with different electric current densities and magnetic fluxes [23].

If a variable magnetic field is applied to the melt, a corresponding electric field is induced in the fluid, and the Lorentz force caused fluid motion to occur [37]. These currents break off dendrite arms and increase nucleation in the same way as mechanical vibration or stirring. This technique is called electromagnetic stirring. Lu et al. [20] found that in hypereutectic Al-Si alloys, electromagnetic stirring implemented at current levels above 12 amps caused the primary silicon particles to congregate, leading to heterogeneity in the microstructure. They found that moderate currents, between 8 and 12 amps, are optimal for refinement. While this refinement of the primary silicon particles is significant, electromagnetic stirring has negligible effects on the eutectic silicon particles. Jung et al. [15] demonstrated this fact in aluminum alloy A356, but also showed that this method could be effectively used in conjunction with chemical modification using strontium to refine both the eutectic particles and the α -Al dendrites.

Another physical method of refinement is the intensive melt shearing process, in which the liquid metal is subjected to intense shearing via a twin screw mechanism prior to use in a high pressure die casting process, as shown schematically in Figure 2.10 [26]. It has been found that this process leads a greater refinement of the primary silicon particles than does chemical modification using phosphorus [25,26]. Zhang et al. [25] speculated that the mechanism of this refinement is the distribution of oxide films as well dispersed nanoscale particles that act as substrates for heterogeneous nucleation.

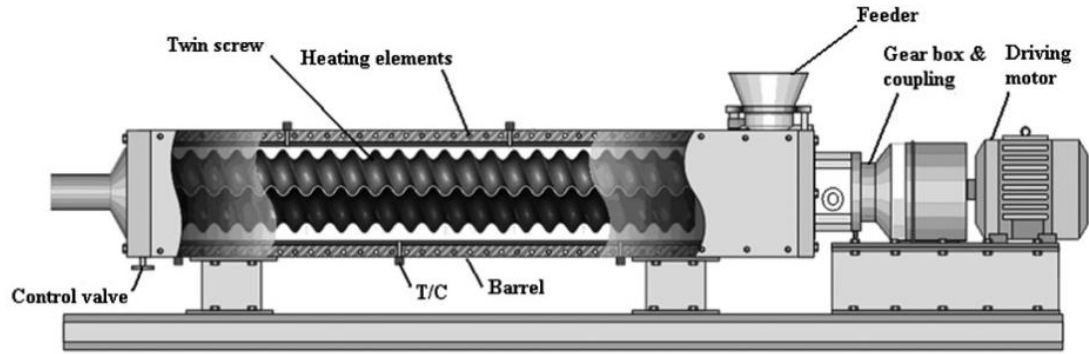


Figure 2.10: Schematic of intensive melt shearing apparatus [26].

2.4. Refinement of Cast Microstructures by an Applied Electric Current

An alternative method for the refinement of cast microstructures is the application of an electric current during solidification. Several early studies theoretically [38] and experimentally [39] investigated the effect of an applied electric current on the segregation and redistribution of solute atoms at a freezing interface during solidification. These studies concluded that electrotransport created by high current densities has a purifying effect on the material and improves segregation. Additionally, because the resistivity of most solid metals is about half that of the liquid phase, significant joule heat generated by the electric current would have the effect of reducing the growth of dendrite arms, with the result of increasing the interfacial stability.

These early studies created an interest in the effect of an applied electric current on the cast microstructure of various materials, and resulted in experimentation being performed by a number of researchers. Among these studies, two distinct regimes of high and low current density can be identified. High current density studies involved the use of

capacitor banks to discharge pulsed current, and low current density studies involved the use of power supplies to apply current in a steady or pulsed manner.

2.4.1. High Electric Current Density Regime

The first studies performed on the effect of electric current on microstructural refinement in the high electric current density regime were performed in the early 1990s on Pb-Sn alloys. Nakada et al. [40] used a capacitor bank to pulse high voltages at 20 second intervals into a hypoeutectic Pb-Sn alloy, also varying the solidification rate and the point during solidification at which the current pulses were applied. Although no quantitative results nor the current densities induced by the capacitor bank were reported, the qualitative results of this experiment showed that the current pulses must be applied during the initial onset of solidification in order to result in modification of the microstructure. In this case, the microstructure was modified from large dendritic grains, to fine globular grains. The proposed mechanism for this refinement was shear stress caused by the pinch force induced by the current pulses. This shear stress caused the dendrites to break into globular fragments. Similar conclusions were reported by Jianming et al. [41], also for a hypoeutectic Pb-Sn alloy. However, Barnak et al's. [42] further experimentation with Pb-Sn alloys showed that the pinch force did not produce high enough stresses to shear dendrite arms. These experiments were performed with electric current densities ranging from 1000-1500 A/cm² applied at frequencies varying from 1.5 to 5 pulses per second. They found that the grain size of the samples were

reduced by approximately an order of magnitude at these values. It was noted that a significant increase in undercooling was observed as a result of the electric current application. It was suggested that the primary effect of the electric current was either a reduction of the free energy difference between the liquid and solid states or an increase in the liquid-solid interfacial energy, resulting in an increased nucleation rate. This conclusion is consistent with the observation by Nakada et al. [40] that the electric current pulses are significantly more effective when applied during the initial stages of solidification.

Qin and Zhou [43] proposed that the mechanism for refinement by pulsed electric current was an increase in the difference in free energy between the solid and liquid states, and that this change in free energy results in an increased nucleation rate. Theoretically, they showed that an electric current can have this effect on the free energy of the system. Numerical calculations were performed that agreed with the results found by Barnak et al. [42], although no direct comparison was made. It was shown that the effect of joule heating, skin effect and pinch force was negligible. The numerical predictions by Qin and Zhou for a variety of pure metals showed that significant refinement should not be possible with electric current densities lower than approximately 10^3 A/cm². However, this conclusion is inconsistent with findings from studies using very low electric current densities [44–48].

Shu-xian et al. performed pulsed electric current studies on A356 aluminum alloys [49][50]. Pulses with electric current densities of approximately 2×10^5 A/cm² were administered at 1.5s periods. The results of these studies showed that the microstructure of the metal was obviously refined when treated with the pulsed electric

current. The authors proposed that the mechanism for refinement was that the pinch force caused by the pulsed electric current broke large nuclei into many smaller nuclei, resulting in more numerous, and thus by necessity, finer grains.

In order to determine the refining mechanism of the high density electric current pulse, Liao et al. [51] performed a systematic study on pure aluminum by applying electric current pulses during the different stages of solidification. They found no change in the solidification structure when the electric pulse was applied to either the high temperature melt or during the grain growth period of solidification. However, significant refinement was observed when the pulse was applied during nucleation. It was concluded that the electric pulse caused nuclei to fall off the mold wall and drift into the liquid, leading to a multiplication of stable nuclei, and that the skin effect greatly enhances this mechanism. This conclusion is consistent with previous speculation that an increased nucleation rate is responsible for the grain refinement [41]. Voltages ranging from 12.5 to 3000 V at frequencies ranging from 100 to 1000 Hz were used, although the corresponding electric current densities were not reported.

Zhang et al. [52] studied the effect of high electric current density pulses on the microstructure of eutectic composition Al-Si alloys. They applied electric current densities ranging from 800 to 2400 A/cm² at 200 Hz. The samples used were cylindrically shaped with diameters of 4 mm and 420 mm in length. The electric current was applied to each sample while being slowly pulled through an electric resistance furnace. They found that the applied electric current created lamellar eutectic structures, as shown in Figure 2.11 The quantity and size of these structures were strongly dependent on electric current density, with a maximum in size and frequency found at

1600 A/cm². Additionally, larger lamellar structures were found for slower pulling rates through the electrical resistance furnace. It was concluded that the applied electric current pulses created local convection currents, driven by the Lorentz force, that supplied solute material to the solidifying lamellar structures. This allowed the structures to grow larger than during solidification without the applied electric current, in which growth would be terminated by localized decreases in silicon content of the fluid feeding the solidifying structure.

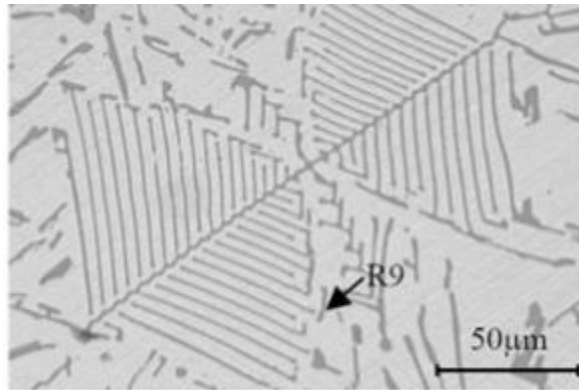


Figure 2.11: Lamellar eutectic structure found after application of high density pulsed electric current to eutectic Al-Si alloy [52].

Xu et al. [53] studied the effect of the application of high density electric current on the microstructure of Al-6.6 wt.% Si alloy, and compared the direct current and alternating current application methods. The electric current used was 220 A, although neither the electric current density, nor the dimensions of the casting necessary to calculate it, were given. They found that the application of the direct current shortened the length of the eutectic silicon particles, and that these particles were preferentially oriented in a particular direction. The orientation direction with respect to the applied

current flow was not reported. When the alternating current was applied, they found numerous small silicon particles dispersed near the large eutectic silicon particles. Figure 2.12 shows examples of these changes in microstructure. Xu et al. attributed this refinement to vibrations induced by the alternating current, similar to that produced using electromagnetic vibration.

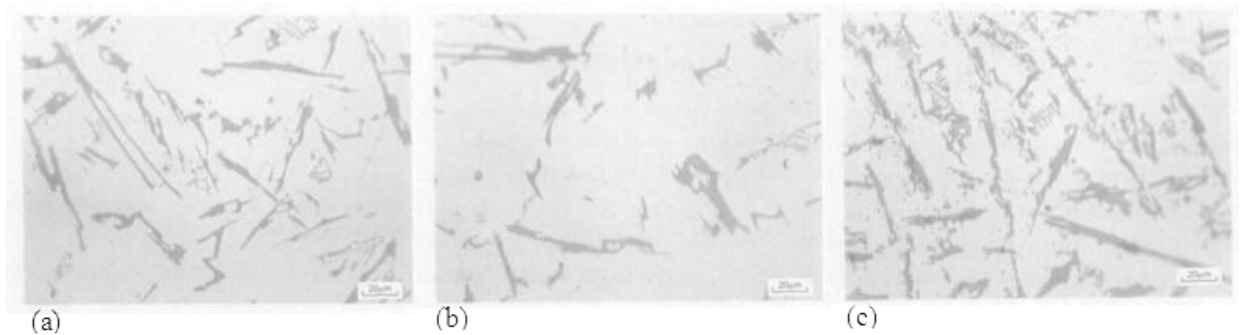


Figure 2.12: Optical photomicrographs of eutectic silicon particles in Al-6.6 wt.% Si alloys without electric current application (a), with direct current application (b), and with alternating current application (c) [53].

Hongsheng et al. [54] conducted a study on hypoeutectic, eutectic, and hypereutectic composition Al-Si piston alloys, and compared the results directly with chemical modification. The charge material was melted using an electric resistance furnace and the current was supplied by a capacitor bank, with a pulsed frequency of 4 Hz, using steel electrodes. Although it was stated that a voltage of 2000V was used, the current density was not discussed. They reported that pulsed electric current refined the α -Al grains as effectively as chemical modification using sodium salt, although their method for grain size measurement was not discussed. In particular, it was shown that the

electric current application had a much greater effect when applied at a higher melt temperature, translating to the nucleation rather than the growth stage of solidification, which agrees with the finding of Liao et al. [51]. It was reported that the eutectic silicon particles in the samples treated with the pulsed current were smaller and more uniform. Figure 2.13 shows an example the change in eutectic silicon particles in an Al-17 wt.% Si alloy as a function of the pulsed electric current. Additionally, the pulsed electric current reduced the size of the primary silicon particles and changed their morphology to more spherical shapes. Figure 2.14 shows SEM photomicrographs of the difference in size of the primary silicon particles with and without the application of the pulsed electric current. Hongsheng et al. concluded that the effect of the electric current on the primary silicon particles was more significant than on the eutectic silicon particles. The effects of the pulsed electric current were more pronounced on alloys with higher silicon content. The tensile strength and microhardness of the alloys were uniformly increased with the application of the electric current.

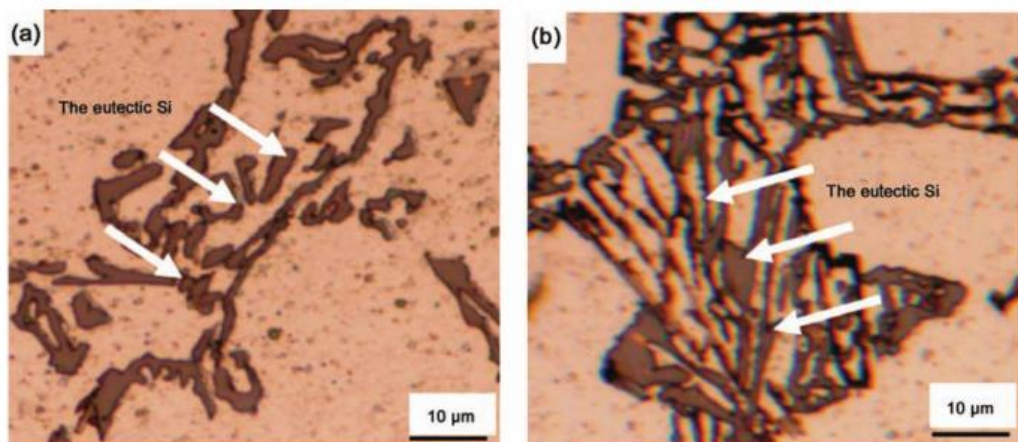


Figure 2.13: Size of eutectic silicon particles in Al-17 wt.% Si with pulsed electric current application (a), and without current application (b) [54].

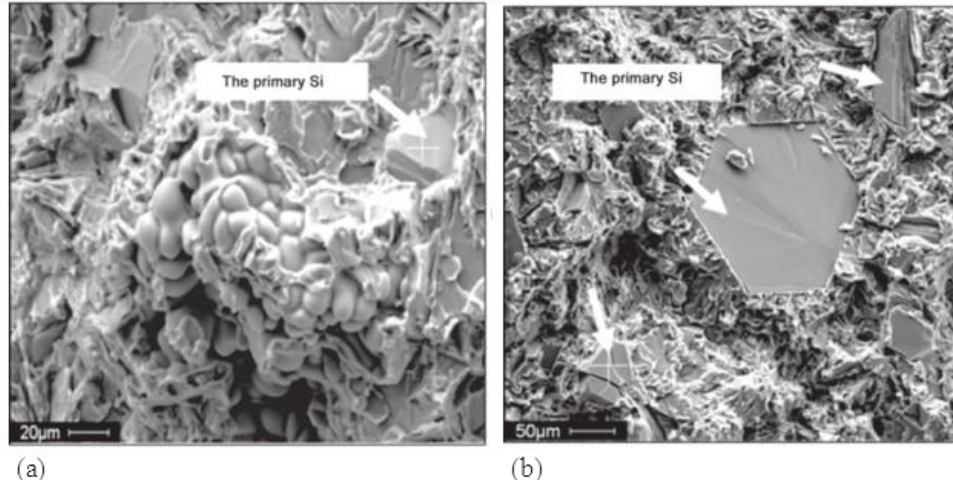


Figure 2.14: SEM photomicrographs showing difference in size of primary silicon particles with applied electric current (a), and without applied electric current (b) [54].

Ban et al. [55] applied high density electric current pulses to hypoeutectic and hypereutectic Al-Si alloys. The alloys used were Al-7 wt.% Si, Al-10 wt.% Si, and Al-22 wt.% Si. The current was applied at 3 kV and 6 kV, with current densities ranging from 2931 A/cm² to 5862 A/cm², respectively. They found that the electric current pulses changed the dendritic structure of the α -Al in the Al-7 wt.% Si from columnar to equiaxed in nature. The electric current shortened the length of the dendrites in the Al-10 wt.% Si alloy, but did not dramatically change their structure. In the Al-22 wt.% Si alloy, the electric current obviously refined the primary silicon particles, and the level of refinement was strongly related to the current density. Figure 2.15 shows optical photomicrographs of the primary silicon particles without the pulsed electric current treatment, and with the treatment at 3 kV and 6 kV. They concluded that the refinement was caused by the pinch force breaking apart solidified dendrite arms or primary silicon

particles. The magnitude of the pinch force is a function of the electric current density, which explains the dependence of the level of refinement on current density.

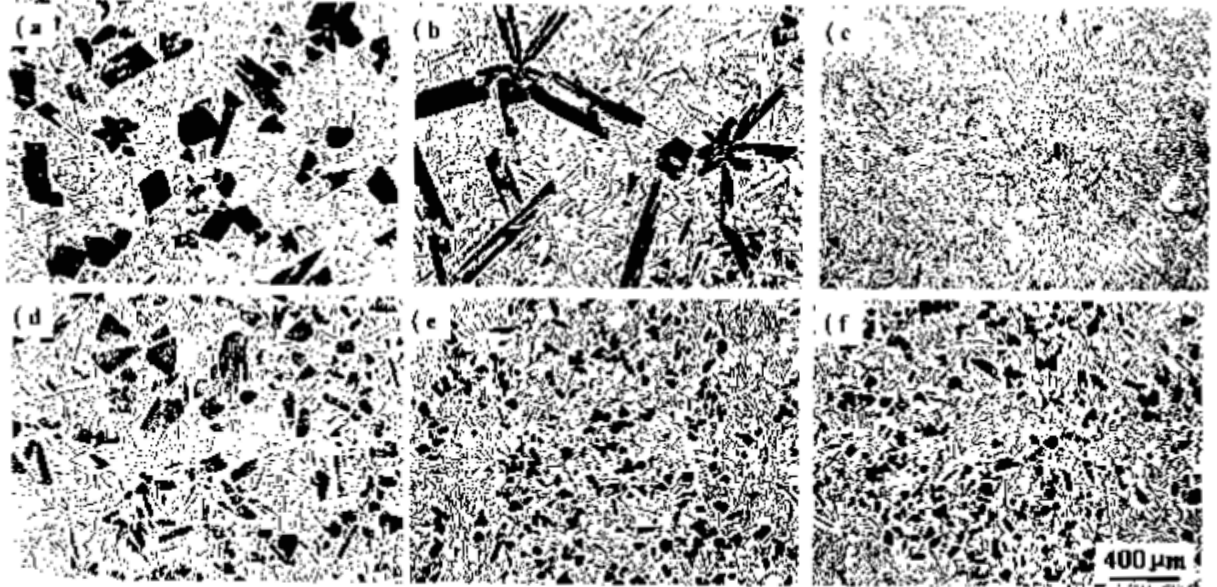


Figure 2.15: Primary silicon particles in Al-22 wt.% Si alloys without pulsed electric current at center of casting (a) and edge of casting (b), with 3 kV pulsed electric current application at center (c), and edge (d) of casting, and with 6 kV of pulsed electric current application at center (e) and edge of casting (f) [55].

2.4.2. Low Electric Current Density Regime

Vaschenko et al. [48] first studied the effect of a steadily applied low density electrical current on the solidification of cast iron. An electric current density of 4-5 mA/cm² was used on samples of varying diameters and the size of the graphite flakes and the bending strength of the samples were measured. They reportedly found that the

application of the electric current refined the graphite flakes in proportion to the cross sectional area of the castings with a maximum reduction in size of 15-40%. Additionally, unrelated to the diameter of the casting, the amount of ferrite was reduced and the amount of pearlite was increased and a decrease in nonmetallic inclusions was also found. An increase in bending strength of 15-20% associated with these changes in microstructure was observed. They speculated that the electric current treatment suppressed nucleation on the impurities in the cast iron, leading to an increase in undercooling and the diffusion of carbon. This leads to an increase in the undercooling and an associated increase in nucleation rate, resulting in a finer microstructure, and higher strength.

Misra [45–47] performed many experiments with direct electric current application during solidification on a number of different of alloys, the first being with Pb-15 wt.% Sb-7 wt.% Sn. An electric current density of 30 to 40 mA/cm² at 30 V in which obvious refinement was found although no quantitative analysis was performed. Similar experimentation, using 50 mA/cm² at 20 V, was then performed on cast iron [56], finding similar results. Misra [45] performed further experimentation with Pb-Sb-Sn alloys and a current density of 50 mA/cm² at 30 V finding consistent refinement and concluded that the refinement was a result of enhanced interface stability caused by joule heating of solidifying perturbations.

Anyalebechi and Tomaswick [44] performed a study on aluminum alloy 7050 with varying solidification rates, electric current densities of 465 and 930 mA/cm² and both steady and pulsed electric current. They found a significant and unambiguous refinement of the cast microstructure in which the average dendrite cell size, average second-phase particle size, average grain size, and the sizes of the largest second-phase

particles were reduced. The proportion of coarse second-phase particles decreased and the distribution of second-phase particle size was more uniform and unimodal. Additionally, it was found that the results were independent of current density, solidification rate, and the type of electric current application, being either pulsed or steady. Figure 2.16 shows polarized light photomicrographs demonstrating the refinement of the dendrite cell size of the 7050 aluminum alloy under all electric current application conditions and over varying solidification rates. The graph in Figure 2.17 shows the decrease in dendrite cell size was not a function of electric current density, or current application method. It was concluded that the mechanism of refinement was primarily due to thermal fluctuations caused by Joule-Thompson and Peltier heating at the base of the dendrite arms, causing the arms to melt off and float into the melt creating additional nuclei. A secondary mechanism was also suggested, being a shear stress induced fragmentation of dendrite arms caused by localized convection currents.

Prodhan showed that the application of electric current can also be used to degas Al-Si alloys during solidification [57,58]. It was found that the dissolved hydrogen was ionized at the anode at the bottom of the melt and then traveled to the cathode at the top of the melt where it is de-ionized and allowed to escape. The degassing procedure using electric current had an efficiency comparable to nitrogen or chlorine-based degassing without the pollution issues caused by chlorine. Figure 2.18 shows the change in hardness of an LM-25 Al-Si alloy as a function of electric current density [57]. The increase in hardness was attributed to the degassing effect of the applied electric current. Changes in hardness for both AC and DC electric currents are shown. It was found that the DC

electric current had a greater effect on the hardness, for a given current density, than the AC current.

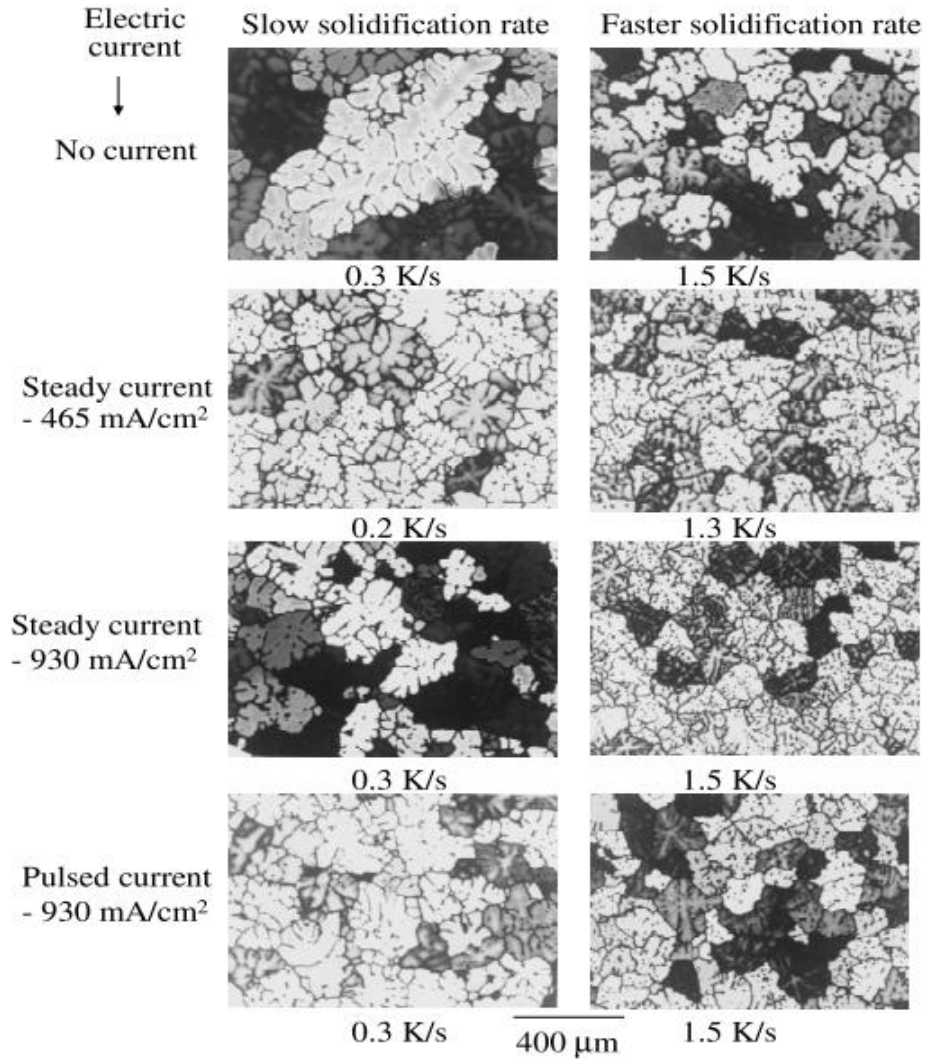


Figure 2.16: Polarized light photomicrographs showing the effect of applied electric current of varying types and electric current densities on the grain size of a 7050 aluminum alloy [44].

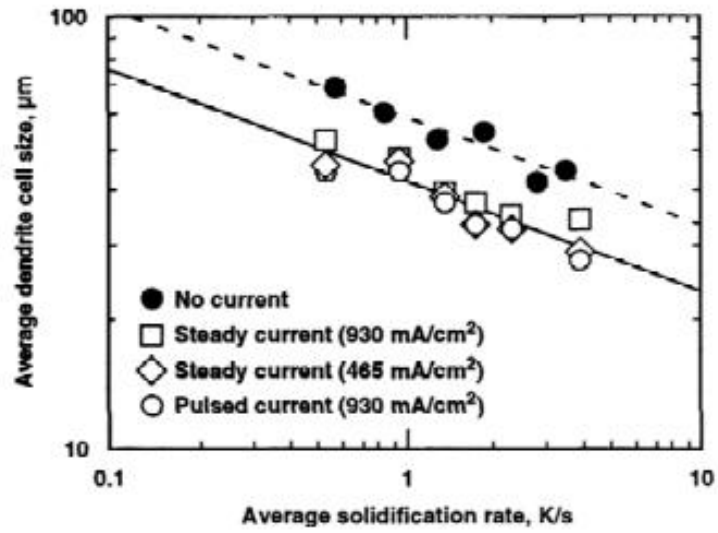


Figure 2.17: Average dendrite cell size as a function of solidification rate for a 7050 type aluminum alloy with and without electric current application [44].

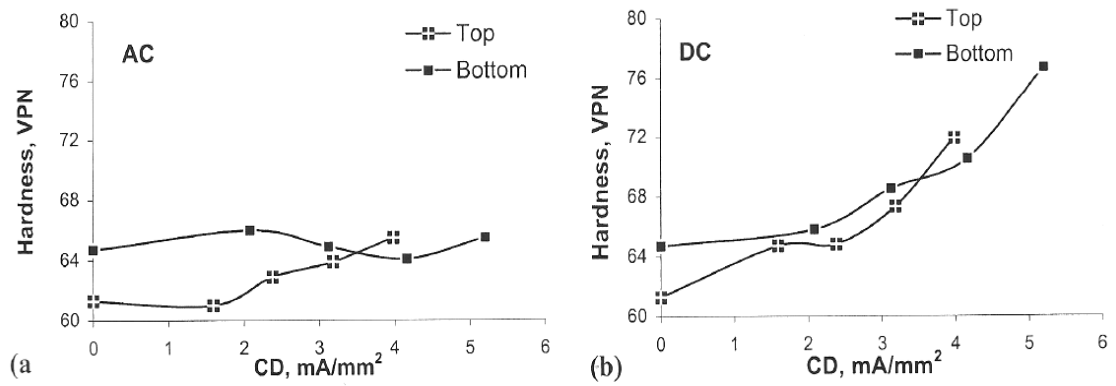


Figure 2.18: Change in hardness of LM-25 Al-Si alloy as a function of electric current density applied in an alternation (a) or direct (b) manner [57].

2.5. References

- [1] S. Hegde and K. N. Prabhu, "Modification of eutectic silicon in Al-Si alloys," *Journal of Materials Science*, Mar. 2008, vol. 43, no. 9, pp. 3009-3027.

- [2] B. K. Prasad, K. Venkateswarlu, O. P. Modi, A. K. Jha, S. Das, and R. Dasgupta, "Sliding Wear Behavior of Some Al-Si Alloys : Role of Shape and Size of Si Particles and Test Conditions," *Metallurgical and Materials Transactions A*, Nov. 1998, vol. 29, pp. 2747-2752.

- [3] A. Clegg and A. Das, "Wear of a Hypereutectic aluminum-silicon alloy," *Wear*, 1977, vol. 43, no. 3, pp. 367-373.

- [4] F. Wang, H. Liu, Y. Ma, and Y. Jin, "Effect of Si content on the dry sliding wear properties of spray-deposited Al-Si alloy," *Materials & Design*, Apr. 2004, vol. 25, no. 2, pp. 163-166.

- [5] T. M. Chandrashekharaiyah and S. a. Kori, "Effect of grain refinement and modification on the dry sliding wear behaviour of eutectic Al-Si alloys," *Tribology International*, Jan. 2009, vol. 42, no. 1, pp. 59-65.

- [6] S. Lim, M. Gupta, Y. Leng, and E. Lavernia, "Wear of a spray-deposited hypereutectic aluminum-silicon alloy," *Journal of Materials Processing Technology*, 1997, vol. 63, pp. 865-870.
- [7] M. Gupta and S. Ling, "Microstructure and mechanical properties of hypo / hyper-eutectic Al-Si alloys synthesized using a near-net shape forming technique," *Journal of Alloys and Compounds*, 1999, vol. 287, pp. 284-294.
- [8] F. Yilmaz and R. Elliott, "The microstructure and mechanical properties of unidirectionally solidified Al-Si alloys," *Journal of Materials Science*, 1989, vol. 24, pp. 2065-2070.
- [9] J. Zhou, J. Duszczek, and B. Korevaar, "Microstructural features and final mechanical properties of the iron-modified Al-20Si-3Cu-1 Mg alloy product processed from atomized powder," *Journal of Materials Science*, 1991, vol. 26, pp. 3041-3050.
- [10] H. S. Dai and X. F. Liu, "Optimal holding temperatures and phosphorus additions for primary silicon refinement in Al-high Si alloys," *Materials Science and Technology*, Oct. 2009, vol. 25, no. 10, pp. 1183-1188.

- [11] K. Nogita, S. D. McDonald, and A. Dahle, "Eutectic Modification of Al-Si Alloys with Rare Earth Metals," *Materials Transactions*, 2004, vol. 45, no. 2, pp. 323-326.
- [12] K. Dahle, K. Nogita, S. D. McDonald, C. Dinnis, and L. Lu, "Eutectic modification and microstructure development in Al-Si Alloys," *Materials Science and Engineering: A*, Dec. 2005, vol. 413-414, pp. 243-248.
- [13] N. Abu-Dheir, M. Khraisheh, K. Saito, and A. Male, "Silicon morphology modification in the eutectic Al-Si alloy using mechanical mold vibration," *Materials Science and Engineering: A*, Feb. 2005, vol. 393, no. 1-2, pp. 109-117.
- [14] X. Jian, T. T. Meek, and Q. Han, "Refinement of eutectic silicon phase of aluminum A356 alloy using high-intensity ultrasonic vibration," *Scripta Materialia*, Mar. 2006, vol. 54, no. 5, pp. 893-896.
- [15] B. I. Jung, C. H. Jung, T. K. Han, and Y. H. Kim, "Electromagnetic stirring and Sr modification in A356 alloy," *Journal of Materials Processing Technology*, 2001, vol. 111, pp. 69-73.
- [16] K. Nogita and A. Dahle, "Effects of boron on eutectic modification of hypoeutectic Al - Si alloys," *Metallurgical Transactions A*, 2003, vol. 48, pp. 307-313.

- [17] J. Y. Chang, G. H. Kim, I. G. Moon, and C. S. Choi, "Rare Earth Concentration in the Primary Si Crystal in Rare Earth Added Al-21wt.%Si Alloy," *Acta Metallurgica*, 1998, vol. 39, no. 3, pp. 307-314.
- [18] C. Chong, L. I. U. Zhong-xia, and R. E. N. Bo, "Influences of complex modification of P and RE on microstructure and mechanical properties of hypereutectic Al-20Si alloy," *Transactions of Nonferrous Metals Society of China*, 2007, vol. 17, pp. 301-306.
- [19] J. Cisse, G. Bolling, and H. Kerr, "Simultaneous Refinement of Primary and Eutectic Silicon in Hypereutectic Al-Si Alloys," *Metallurgical Transactions B*, Mar. 1975, vol. 6, pp. 195-197.
- [20] D. Lu, Y. Jiang, G. Guan, R. Zhou, Z. Li, and R. Zhou, "Refinement of primary Si in hypereutectic Al-Si alloy by electromagnetic stirring," *Journal of Materials Processing Technology*, Jul. 2007, vol. 189, no. 1-3, pp. 13-18.
- [21] F. C. Robles Hernández and J. H. Sokolowski, "Comparison among chemical and electromagnetic stirring and vibration melt treatments for Al-Si hypereutectic alloys," *Journal of Alloys and Compounds*, Dec. 2006, vol. 426, no. 1-2, pp. 205-212.

- [22] K. Sukumaran, B. . Pai, and M. Chakraborty, “The effect of isothermal mechanical stirring on an Al–Si alloy in the semisolid condition,” *Materials Science and Engineering: A*, Mar. 2004, vol. 369, no. 1–2, pp. 275-283.
- [23] J. Yu, Z. Ren, and K. Deng, “Refinement and migrating behaviors in Al-Si hypereutectic alloys solidified under electromagnetic vibration,” *Acta Metallurgica Sinica*, 2011, vol. 24, no. 4, pp. 301-308.
- [24] A. Radjai, K. Miwa, and T. Nishio, “An Investigation of the Effects Caused by Electromagnetic Vibrations in a Hypereutectic Al-Si Alloy Melt,” *Metallurgical and Materials Transactions A*, May 1998, vol. 29, pp. 1477-1484.
- [25] Z. Zhang, H.-T. Li, I. C. Stone, and Z. Fan, “Refinement of primary Si in hypereutectic Al-Si alloys by intensive melt shearing,” *IOP Conference Series: Materials Science and Engineering*, Jan. 2012, vol. 27, pp. 1-6.
- [26] N. S. Barekar, B. K. Dhindaw, and Z. Fan, “Improvement in silicon morphology and mechanical properties of Al–17Si alloy by melt conditioning shear technology,” *International Journal of Cast Metals Research*, Aug. 2010, vol. 23, no. 4, pp. 225-230.
- [27] D. P. Kanicki, “Processing molten aluminum - part 1 : understanding silicon modification,” *Modern Casting*, Jan. 1990, p. 24.

- [28] K. Nogita, J. Drennan, and A. Dahle, "Evaluation of Silicon Twinning in Hypo-Eutectic Al – Si Alloys," *Materials Transactions*, 2003, vol. 44, no. 4, pp. 625-628.
- [29] P. Shingu and J.-I. Takamura, "Grain-Size Refining of Primary Crystals in Hypereutectic Al-Si and Al-Ge Alloys," *Metallurgical Transactions*, Aug. 1970, vol. 1, pp. 2339-2340.
- [30] S. Shankar, Y. W. Riddle, and M. Makhlof, "Eutectic Solidification of Aluminum- Silicon Alloys," *Metallurgical and Materials Transactions A*, Sep. 2004, vol. 35, pp. 3038-3043.
- [31] X. Liu, Y. Wu, and X. Bian, "The nucleation sites of primary Si in Al–Si alloys after addition of boron and phosphorus," *Journal of Alloys and Compounds*, Apr. 2005, vol. 391, no. 1–2, pp. 90-94.
- [32] J. Chang and I. Moon, "Refinement of cast microstructure of hypereutectic Al-Si alloys through the addition of rare earth metals," *Journal of Materials Science*, 1998, vol. 33, pp. 5015-5023.
- [33] M. P. Cicco, L.-S. Turng, X. Li, and J. H. Perepezko, "Nucleation Catalysis in Aluminum Alloy A356 Using Nanoscale Inoculants," *Metallurgical and Materials Transactions A*, Jan. 2011, vol. 42, no. 8, pp. 2323-2330.

- [34] H. Choi, H. Konishi, and X. Li, "Al₂O₃ nanoparticles induced simultaneous refinement and modification of primary and eutectic Si particles in hypereutectic Al–20Si alloy," *Materials Science and Engineering: A*, Apr. 2012, vol. 541, pp. 159-165.
- [35] W. Kasprzak, M. Sahoo, J. Sokolowski, H. Yamagata, and H. Kurita, "The Effect of the Melt Temperature and the Cooling Rate on the Microstructure of the Al-20% Si Alloy Used for Monolithic Engine Blocks," *International Journal of Metalcasting*, Summer 2009, pp. 55-72.
- [36] F. Taghavi, H. Saghafian, and Y. H. K. Kharrazi, "Study on the effect of prolonged mechanical vibration on the grain refinement and density of A356 aluminum alloy," *Materials & Design*, May 2009, vol. 30, no. 5, pp. 1604-1611.
- [37] H. K. Moffatt, "Electromagnetic Stirring," *Physics of Fluids A*, May 1991, vol. 3, pp. 1336-1343.
- [38] J. Angus, D. Ragone, and E. Hucke, "The Effect of an Electric Field on the Segregation of Solute Atoms at a Freezing Interface," in *Metallurgical Society Conference*, 1961, pp. 833-843.

- [39] J. Verhoeven, "The Effect of an Electric Field upon the Solidification of Bismuth-Tin Alloys," *Transactions of the Metallurgical Society of AIME*, Jun. 1965, vol. 233, pp. 1156-1163.
- [40] M. Nakada, Y. Shiohara, and M. Flemings, "Modification of Solidification Structures by Pulse Electric Discharging," *ISIJ International*, 1990, vol. 30, no. 1, pp. 27-33.
- [41] L. Jianming, L. Shengli, and L. Hantong, "Modification of Solidification Structure by Pulse Electric Discharging," *Scripta metallurgica et materialia*, 1994, vol. 31, no. 12, pp. 1691-1694.
- [42] J. Barnak and A. Sprecher, "Colony (grain) size reduction in eutectic Pb-Sn castings by electroplusing," *Scripta metallurgica et materialia*, 1995, vol. 32, no. 6, pp. 879-884.
- [43] R. Qin and B. Zhou, "Effect of Electric Current Pulses on Grain Size in Castings," *International Journal of non-Equilibrium Processing*, 1998, vol. 11, pp. 77-86.
- [44] P. N. Anyalebechi and K. M. Tomaswick, "Effect of Application of Electric Current During Solidification on the Cast Microstructure of Aluminum Alloy 7050," in *EPD Congress 2009*, 2009, pp. 541-554.

- [45] A. Misra, "Effect of Electric Potentials on Solidification of Near Eutectic Pb-Sb-Sn Alloy," *Materials Letters*, 1986, vol. 4, no. 3, pp. 176-177.
- [46] A. Misra, "Misra Technique Applied to Solidification of Cast Iron," *Metallurgical Transactions A*, Feb. 1986, vol. 16, pp. 358-360.
- [47] A. K. Misra, "A Novel Solidification Technique of Metals and Alloys : Under the Influence of Applied Potential," *Metallurgical Transactions A*, Jul. 1985, vol. 24, pp. 1354-1355.
- [48] K. Vashchenko, D. Chernega, S. Vorob'ev, N. Lysenko, and Y. Yakovchuk, "Effect of Electric Current on the Solidification of Cast Iron," *Metallovedenie i Termicheskaya Obrabotka Metallov*, Mar. 1974, vol. 3, pp. 62-65.
- [49] H. Shu-xian, W. Jun, S. Bao-de, and Z. Yao-he, "Effect of high density pulse electric current on solidification structure of low temperature melt of A356 alloy," *Transactions of Nonferrous Metals Society of China*, 2002, vol. 12, no. 3, pp. 414-418.
- [50] H. Shu-xian, W. Jun, J. Wan, S. Bao-de, and Z. Yao-he, "Effect of melt pulse electric current and thermal treatment on A356 alloy," *Transactions of Nonferrous Metals Society of China*, 2003, vol. 13, no. 1, pp. 126-130.

- [51] X. Liao, Q. Zhai, J. Luo, W. Chen, and Y. Gong, "Refining mechanism of the electric current pulse on the solidification structure of pure aluminum," *Acta Materialia*, May 2007, vol. 55, no. 9, pp. 3103-3109.
- [52] Y. Zhang et al., "Influence of Electric-Current Pulse Treatment on the Formation of Regular Eutectic Morphology in an Al-Si Eutectic Alloy," *Metallurgical and Materials Transactions B*, mar. 2011, vol. 42, no. 3, pp. 604-611.
- [53] G. Xu, J. Zheng, Y. Liu, and J. Cui, "Effect of electric current on the cast microstructure of Al-Si alloy," *China Foundry*, 2005, vol. 2, no. 3, pp. 171-175.
- [54] D. Hongsheng, Z. Yong, J. Sanyong, C. Ruirun, and Z. Zhilong, "Influences of pulse electric current treatment on solidification microstructures and mechanical properties of Al-Si piston alloys," *China Foundry*, 2008, vol. 6, no. 1, pp. 24-31.
- [55] C. Ban, Y. Han, Q. Ba, and J. Cui, "Influence of Pulse Electric Current on Solidification Structures of Al-Si Alloys," *Materials Science Forum*, 2007, vol. 546-549, pp. 723-728.
- [56] A. Misra, "Misra Technique Applied to Solidification of Cast Iron," *Metallurgical Transactions A*, Feb. 1986, vol. 17, pp. 358-360.

- [57] A. Prodhan, "A Method for Degassing and Microstructural Modifications of Aluminum Alloys by Electric Current Treatment," *American Foundry Society Transactions*, 2008, pp. 233-246.
- [58] A. Prodhan, "Effect of Electric Current (Plasma) Treatment on LM-6 Al-Si Alloy," *American Foundry Society Transactions*, 2009, pp. 63-77.

Chapter 3

Experimental Work

3.1. Introduction

In order to assess the effect of an applied electric current during solidification on the microstructure of hypereutectic Al-Si alloys, an experimental method was developed to make castings with and without the application of electric current. The following sections detail the experimental setup and procedure used for this study.

3.2. Casting Process Selection and Mold Design

In deciding which casting process to use for this work, consistency from casting to casting, and the ease of altering the process to easily include thermocouples and electrodes were of primary importance. For the purposes of consistency between castings and the ease of altering the setup for thermocouples and changing over from between experimental conditions, a permanent mold process was selected. Additionally, this type of process was simple to implement using the foundry equipment available at GVSU.

In designing the geometry of the mold and what material the mold should be made from, the following considerations were of primary importance:

- i. A mold material with an electrical conductivity lower than that of the aluminum alloys being cast, but with high thermal conductivity to provide sufficient solidification rates
- ii. Ease of fabrication of the mold
- iii. Cost of mold material

The first decision made was to cast flat plates, rather than a cylindrical geometry as is common in the literature [1–3]. The designed casting shape was 177.8 mm long, 101.6 mm wide, and 25.4 mm thick. Figure 3.1 shows the general shape of the mold including three holes that were drilled to allow access of thermocouples for temperature measurement during solidification. The design includes holes for two dowel pins in order to locate the two halves of the mold to each other.

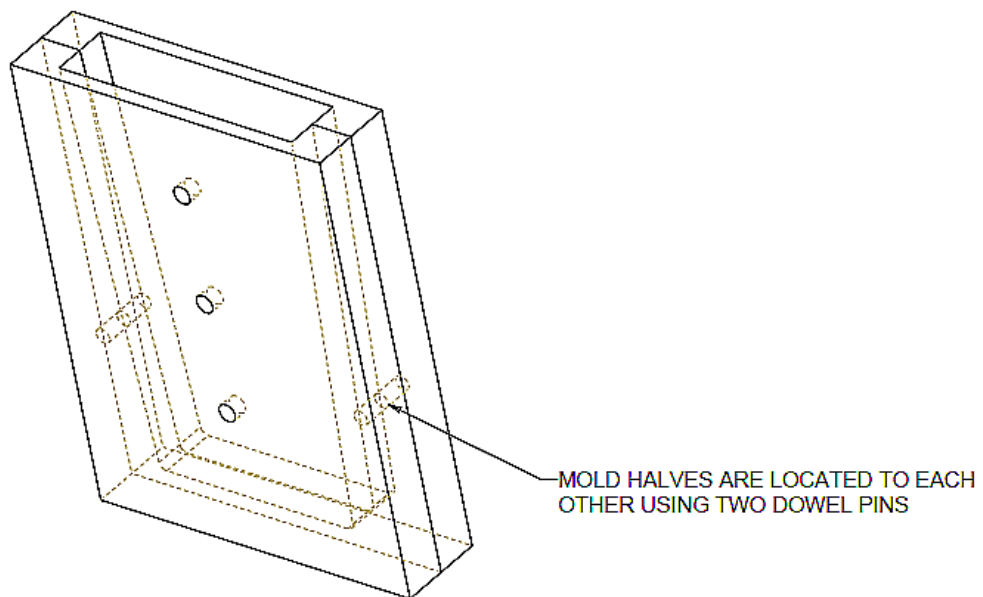


Figure 3.1: Mold machined from mild steel. The two halves of the mold were located to each other using dowel pins.

A ceramic mold was considered for that class of materials' extremely low electric conductivity. However, ceramics also have low thermal conductivities and a ceramic mold would have created unacceptably low solidification rates in addition to being expensive and difficult to fabricate. A metallic mold (mild steel) was chosen for its low cost and good machinability, while still having an electrical conductivity approximately an order of magnitude smaller than that of aluminum and good thermal conductivity properties. The two halves of the mold were machined from flat stock using a HAAS CNC milling machine.

3.3. Rationale for Choice of Experimental Conditions

The experimental conditions for this work were carefully chosen and evaluated. These considerations included the alloy compositions that were used, the method of applying the electric current, and the details of the casting procedure.

3.3.1. Alloy Composition

Three different hypereutectic alloy compositions were provided courtesy of ALCOA Inc.: Al-13 wt.% Si, Al-20 wt.% Si, and Al-30 wt.% Si. Originally, it was intended to investigate the effect of the electric current on both the eutectic and primary silicon particles, as well as to assess the change in any effect as a function of the composition of the alloy. As can be seen in the Al-Si phase diagram in Figure 3.2, the

eutectic composition for this system is 12.6 wt.% Si. As such, the Al-13 wt.% Si alloy was ideal for studying the refinement of the eutectic particles as the microstructure in this alloy almost entire composed of the eutectic structure. The 20 wt.% was used to investigate the effect of the electric current on the primary silicon particles. Originally, it was planned to use the Al-30 wt.% Si alloy in conjunction with the Al-20 wt.% Si alloy to assess the effect of silicon content on refinement of the primary particles. However, due to time constraints, no castings of the Al-30 wt.% Si alloy were made. As such, compositions effect were not investigated.

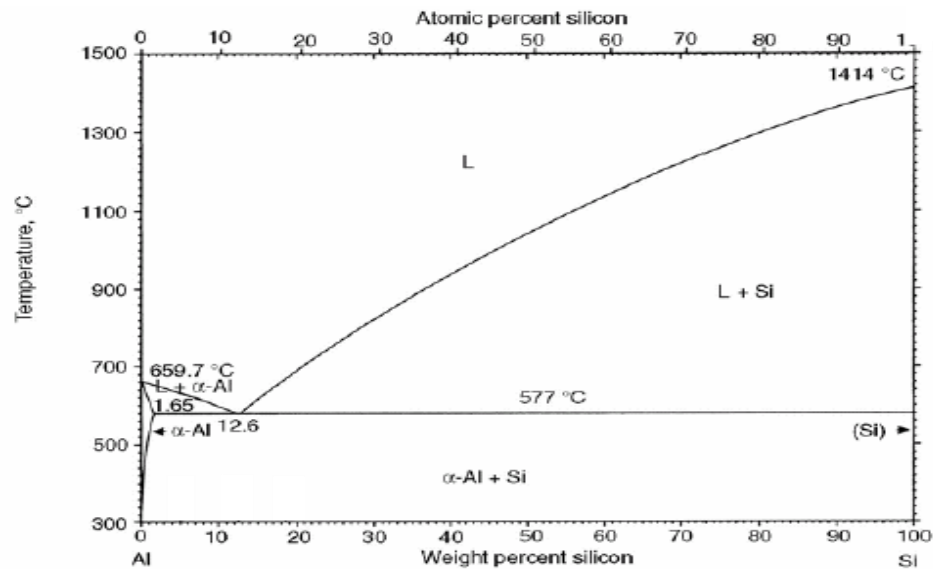


Figure 3.2: The Al-Si phase diagram.

3.3.2. Casting Shape and Size

The permanent mold casting process was selected in part because of the casting to casting consistency. Several preliminary castings were made with scrap aluminum

(mostly 6061 and A356 alloys) to assess shrinkage. The castings conformed well to the shape of the mold and contained only minimal shrinkage on the top surface and near the thermocouple locations.

3.3.3. Thermocouple Design, Placement, and Data Collection

K type chromel-alumel thermocouples were used for this experimentation and were made from 32 gauge (0.202 mm diameter) insulated wire. A relatively large gauge was used so that the thermocouple beads could withstand the conditions during casting, although this sacrifices the faster response time of smaller gauges. Near the tip of each thermocouple, a ceramic sleeve was used to protect the bare wire from the casting environment, while leaving just the thermocouple bead exposed, as Figure 3.4 shows.



Figure 3.4: K type thermocouple with ceramic sleeve used for temperature measurement during solidification.

The thermocouples were evenly spaced in the casting as shown in Figure 4.5. Using this arrangement, the variation of solidification time with position could be evaluated. Prior to casting, the thermocouples were held in place using a thermoplastic adhesive on the outer surface of the mold. A National Instruments cDAQ-9172 Chassis and NI9211 module were used for data acquisition in conjunction with SignalExpress software. In all of the experiments, data were collected at a rate of 2 Hz. Figure 3.5 shows the location of each of the thermocouples and the appropriate channels they were connected to for data collection.

3.3.4. Electric Current Application

The electrodes were selected based on electrical conductivity, melting temperature, cost, and ease of use. Conductive graphite rods were selected based upon their low cost, high melting temperature, that they could be readily ordered in standard, usable lengths and diameters, and have been previously used for similar experimentation [1].

The electric current was applied using two 6.35 mm diameter conductive graphite rods as electrodes. A constant voltage power supply was used to supply the current and a power resistor was added to the circuit to avoid shorting the power supply. The electric current was applied in a steady manner, as is common in the literature for similar low electric current density studies [1,3,4]. The electrodes were press-fitted into wooden blocks to hold them in place and insulate them from the mold prior to pouring. Figure 3.6

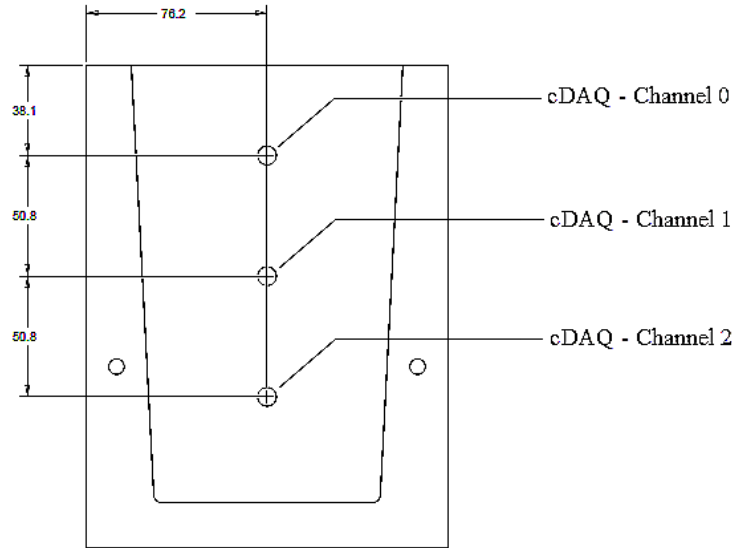


Figure 3.5: Engineering drawing of mold showing thermocouple placement (dimensions in mm) and the corresponding data acquisition channel for each.

shows a schematic of the electrode setup. During each experiment in which the current was applied, the voltage was read from the power supply display and the resistance of the circuit was measured using a digital multi-meter once solidification had been completed. Ohm's law was then used to calculate the current flowing through the casting. These calculations were performed assuming that the electrical conductivity of the Al-Si alloy did not change significantly between the solid and liquid phases. This assumption is not completely accurate, and because the resistivity of the liquid phase is generally higher than that of the solid phase, this calculation will slightly underestimate the current density when the casting is in the liquid and mushy regions. The power supply was activated prior to pouring, when the electrodes were not connected. The circuit was then completed by the liquid metal during pouring, ensuring that current was passed through the casting as soon as the liquid metal contacted the electrodes. Temperature was monitored in real

time during the casting process. Using this information as an indicator of the solidification process, the electric current was shut off once it was apparent that the material surrounding all three thermocouple locations was completely solid. Figure 3.7 shows a photograph of the electrode setup, and Figure 3.8 shows a photograph of the power supply used to apply the electric current.

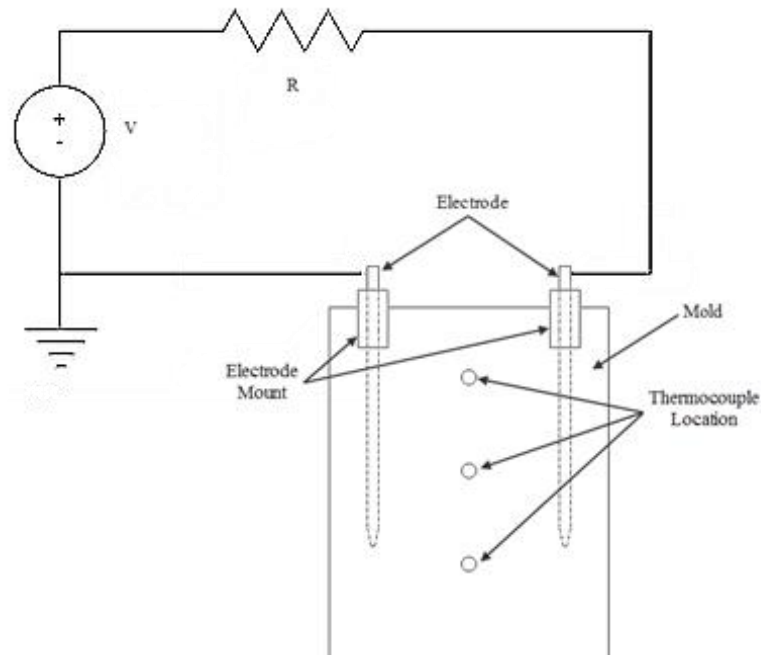


Figure 3.6: Schematic of electrode setup.



Figure 3.7: Photograph of the electrode setup at the mold prior to pouring.



Figure 3.8: Photograph of the power supply used to apply the electric current.

3.3.5 Casting Conditions

In preliminary castings, a temperature drop of about 100 °C was observed between the furnace and the mold. This large change in temperature was likely a function of the long response time of the thermocouple measurements and the fast solidification rates immediately after pouring, caused by chilling of the mold walls and thermocouples. To account for the response time of the thermocouples, the temperature of the melt in the furnace was increased by 100 °C. With a desired superheat of 50 °C, this equates to a melt temperature 150 °C above the liquidus temperature for the composition in question. For the Al-20 wt.% Si alloy, with a liquidus temperature of 700 °C, a melt temperature of

850 °C was used. A melt temperature of 825 °C was used for the Al-13 wt.% Si alloy castings.

3.4. Preparation of Cast Ingots

The charge material was melted in a graphite crucible using a natural gas furnace and pouring was performed manually. The melt was not degassed. For each casting, 1.3 - 1.5 kg of charge material was used. The inside of the mold was coated with parting dust prior to each to ensure easy removal of the finished castings. The casting process, from removing the crucible from the furnace to completing the pouring of the material into the mold, lasted approximate one minute and the finished casting was left overnight and allowed to air cool. During the casting procedure, the mold was buried in casting sand, as shown in Figure 3.7, in order to protect the thermocouple wires and to contain any spills or leakage during pouring. Melt temperature prior to pouring was monitored using an additional k-type thermocouple connected to a digital multi-meter. Figure 3.9 shows the furnace and foundry equipment used for pouring of the molten metal.

Two castings were made for each case, being with and without an applied electric current and for each alloy. Table 3.1 shows the parameters of each experiment performed with the Al-20 wt.% Si alloy, and Table 3.2 shows the parameters for each casting made with the Al-13 wt.% Si alloy. The current density values are simply computed as shown in Equation 3.1.

$$i = \frac{I}{A} \quad (3.1)$$

where i is current density, I is the current applied to the casting, and A is the cross-sectional area of the casting normal to the direction of current flow. This calculation is valid assuming that the current is spread evenly across the cross-sectional area of the aluminum casting, and does not flow through the steel mold. The latter assumption is based on the fact that the electrical conductivity of aluminum is approximately an order of magnitude greater than that of mild steel.

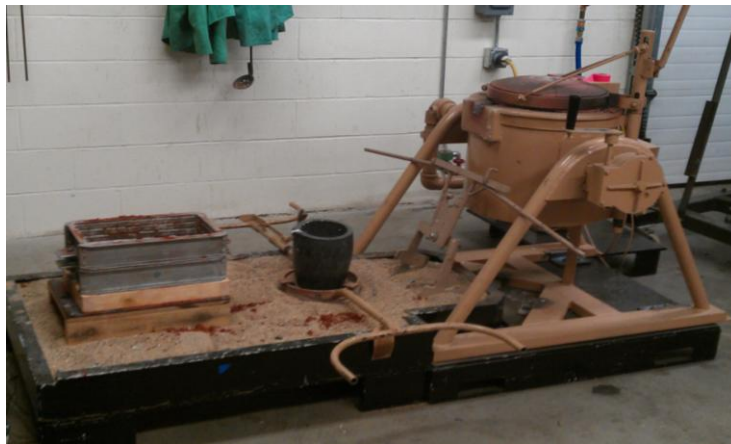


Figure 3.9: Mifco T-160 furnace and foundry equipment.

Table 3.1: Experimental parameters or Al - 13wt.% Si castings with applied current.

Experimental Parameter	Casting G	Casting H
Initial Casting Temperature (°C)	856	851
Resistor Used	3 Ω, 100 W	4.5 Ω, 1000 W
Measured Resistance of Circuit (Ω)	4.05	4.7
Applied Voltage (V)	85	110
Calculated Current (A)	20.98	23.4
Current Density (mA/cm ²)	465	518

Table 3.2: Experimental parameters for Al - 20 wt.% Si castings with applied current.

Experimental Parameter	Casting C	Casting D
Initial Casting Temperature (°C)	826	825
Resistor Used	4.5 Ω, 1000 W	4.5 Ω, 1000 W
Measured Resistance of Circuit (Ω)	4.85	5.17
Applied Voltage (V)	110	110
Calculated Current (A)	22.7	21.3
Current Density (mA/cm ²)	502	471

3.5. Characterization of the Cast Ingot Microstructures

From each finished casting, a sample was taken from material surrounding each of the thermocouples. By doing this, it could be safely assumed that the temperature recorded by the thermocouple was representative of the conditions that produced the microstructure in the corresponding sample. The surface of each sample that was nearest the bottom of the casting was metallographically prepared. Figure 3.10 shows how each sample was cut around the thermocouples and labels which surface was used for metallographic preparation. Figure 3.11 shows two examples of cast ingots with the thermocouples imbedded in the cast material. Figure 3.12 shows a photograph of the completed and assembled mold.

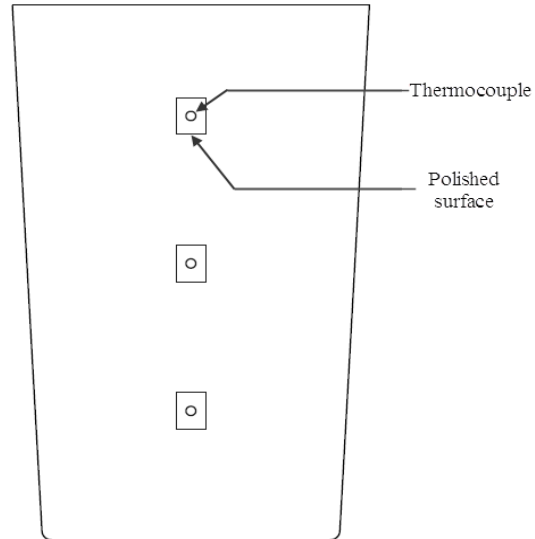


Figure 3.10: Schematic showing how each sample was cut around one of the thermocouples and the surface that was metallographically prepared.

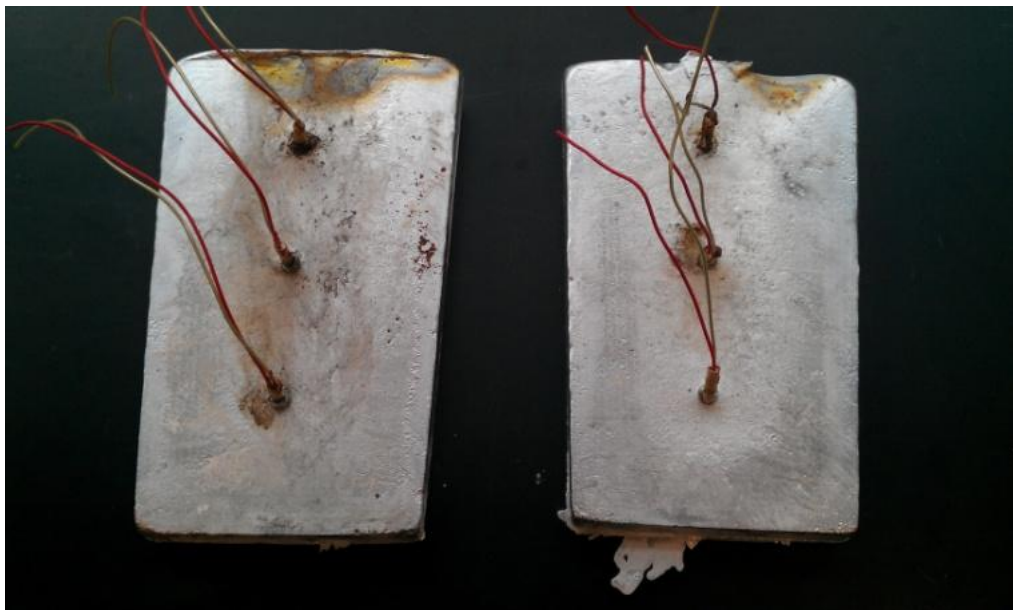


Figure 3.11: Example of cast ingots with thermocouples imbedded in castings.



Figure 3.12: Photograph of completed and assembled mold.

3.6. References

- [1] P. N. Anyalebechi and K. M. Tomaswick, "Effect of Application of Electric Current During Solidification on the Cast Microstructure of Aluminum Alloy 7050," in *EPD Congress 2009*, 2009, pp. 541-554.
- [2] A. Misra, "Effect of Electric Potentials on Solidification of Near Eutectic Pb-Sb-Sn Alloy," *Materials Letters*, 1986, vol. 4, no. 3, pp. 176-177.
- [3] A. Misra, "Misra Technique Applied to Solidification of Cast Iron," *Metallurgical Transactions A*, Feb. 1986, vol. 16, pp. 358-360.

- [4] K. Vashchenko, D. Chernega, S. Vorob'ev, N. Lysenko, and Y. Yakovchuk,
“Effect of Electric Current on the Solidification of Cast Iron,” *Metallovedenie i
Termicheskaya Obrabotka Metallov*, Mar. 1974, vol. 3, pp. 62-65.

Chapter 4

Results and Discussion

4.1. Introduction

The data collected from this study are of three types: (i) quantitative temperature measurements from each casting, (ii) optical photomicrographs from each sample, and (iii) quantitative measurements of dendrite cell size from each sample. The temperature data was used to calculate local solidification times and rates and comparisons of these values were made for corresponding location in castings solidified with and without the application of electric current.

4.2. Local Solidification Rates

Cooling curves were constructed using the temperature-time data obtained with the thermocouples in each casting. Figure 4.1 shows overlaid cooling curves for two of the Al-13wt.% Si castings; one with, and one without the electric current treatment. The same is shown for two of the Al-20wt.% Si casting in Figure 4.2 From these graphs, it is apparent that there were no significant differences in solidification time for castings with and without the applied electric current.

Using the temperature data, the local solidification times and solidification rates for each location in each casting were calculated. Solidification rate was calculated using Equation (4.1).

$$\dot{T} = \frac{\Delta T}{\Delta t} \quad (4.1)$$

where \dot{T} is local solidification rate, ΔT is the freezing range, and Δt is the local solidification time. The local solidification times and calculated solidification rates are shown in Table 4.1.

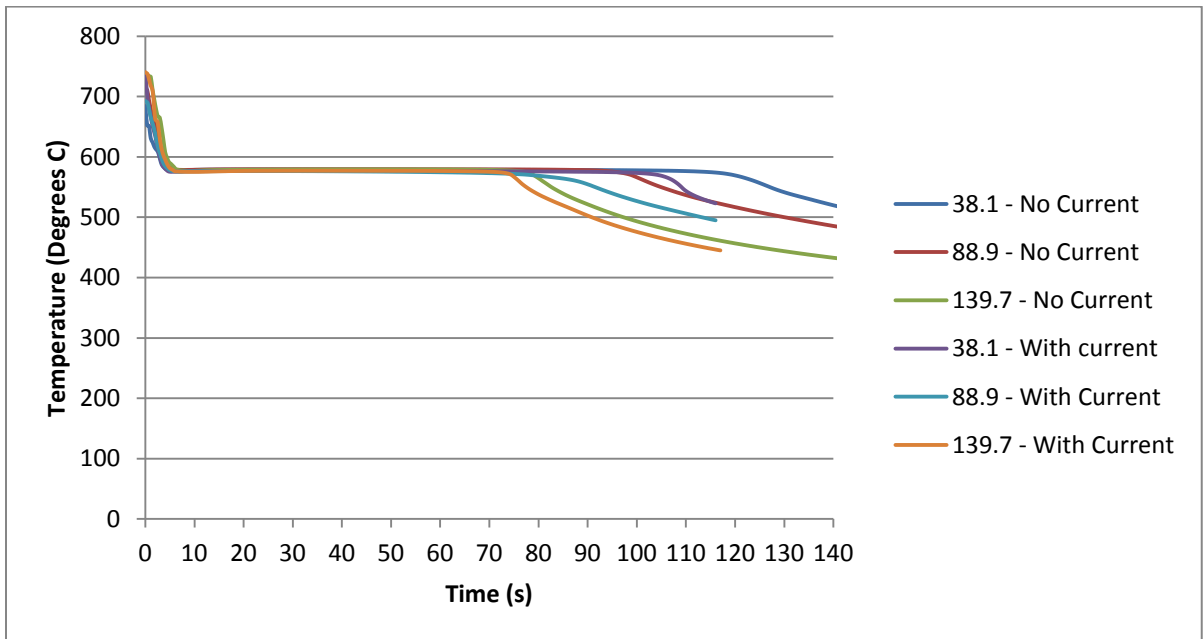


Figure 4.1: Comparison of cooling curves for Al-13 wt.% Si without and with electric current treatment as a function of distance (in mm) from the top of the mold.

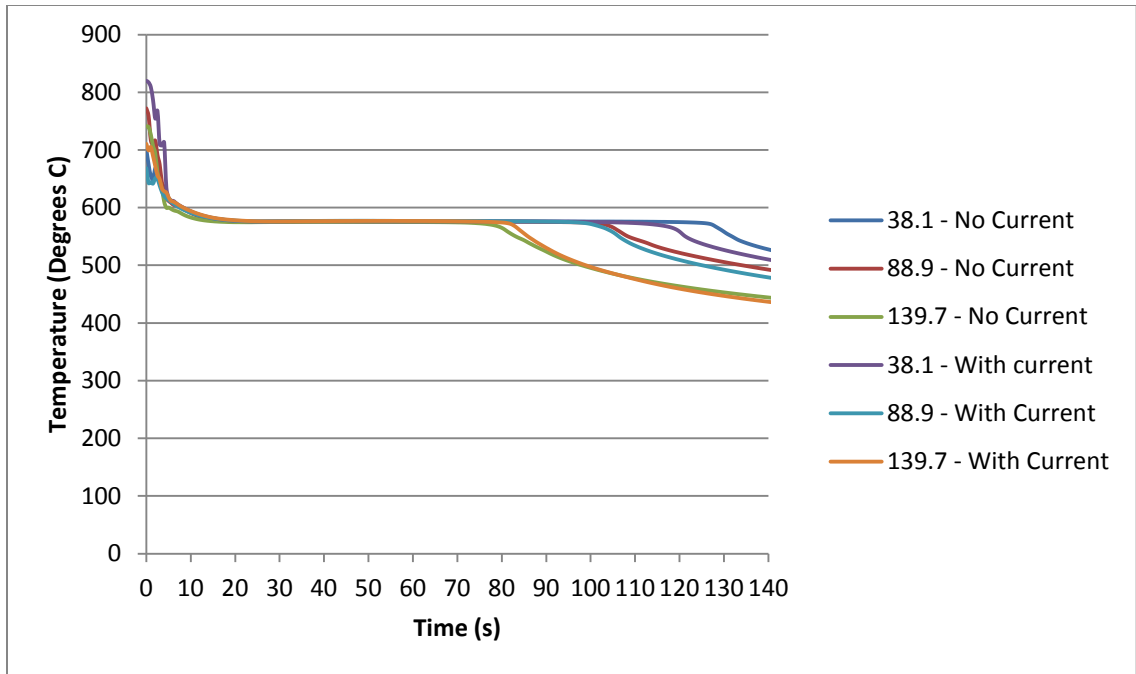


Figure 4.2: Comparison of cooling curves for Al-20 wt.% Si without and with electric current treatment as a function of distance (in mm) from the top of the mold.

Figure 4.3 shows the local solidification rate in each casting as a function of distance from the top of the cast ingot. For each composition, the local solidification rates at each location are very similar between castings.

4.3. Cast Microstructure

In general, the cast microstructure of the castings of both hypereutectic Al-Si alloys produced with and without application of electric current during solidification consisted of primary silicon particles, eutectic silicon particles, and eutectic aluminum dendrite cells. The volume fraction of these phases depended on the silicon content of the

Table 4.1: Local solidification times and solidification rates for Al-13 wt.% Si castings.

Composition	Casting	Condition	Distance From Top of Mold (mm)	Local Solidification Time (s)	Local Solidification Rate ($^{\circ}\text{C/s}$)
Al-13 wt.% Si	A	No Current	38.1	105	0.08
			88.9	86	0.09
			139.7	66	0.12
	B	No Current	38.1	101	0.08
			88.9	86	0.09
			139.7	70	0.12
	C	502 mA/cm ²	38.1	96	0.08
			88.9	69	0.12
			139.7	67	0.12
	D	471 mA/cm ²	38.1	102	0.08
			88.9	82	0.10
			139.7	63	0.13
Al-20 wt.% Si	E	No Current	38.1	104	1.09
			88.9	99	1.15
			139.7	75	1.52
	F	No Current	38.1	121	0.93
			88.9	94	1.20
			139.7	70	1.61
	G	465 mA/cm ²	38.1	116	0.98
			88.9	107	1.06
			139.7	73	1.55
	H	518 mA/cm ²	38.1	102	1.11
			88.9	95	1.20
			139.7	75	1.52

alloy. The cast microstructure of the Al-13 wt.% Si alloy consisted primarily of eutectic silicon particles and eutectic aluminum dendrite cells, with a small volume fraction of primary silicon particles. The primary silicon particles in this alloy tend to be small and not faceted. Figure 4.4 shows an optical photomicrograph of the Al-13 wt.% Si cast

microstructure. The cast microstructure of the Al-20 wt.% Si alloy included a much larger volume fraction of primary silicon particles, and a correspondingly smaller quantity of eutectic silicon particles and eutectic aluminum dendrite cells. The primary silicon particles in this alloy were much larger and tended to be faceted. Figure 4.5 shows an optical photomicrograph of the Al-20 wt.% Si cast microstructure.

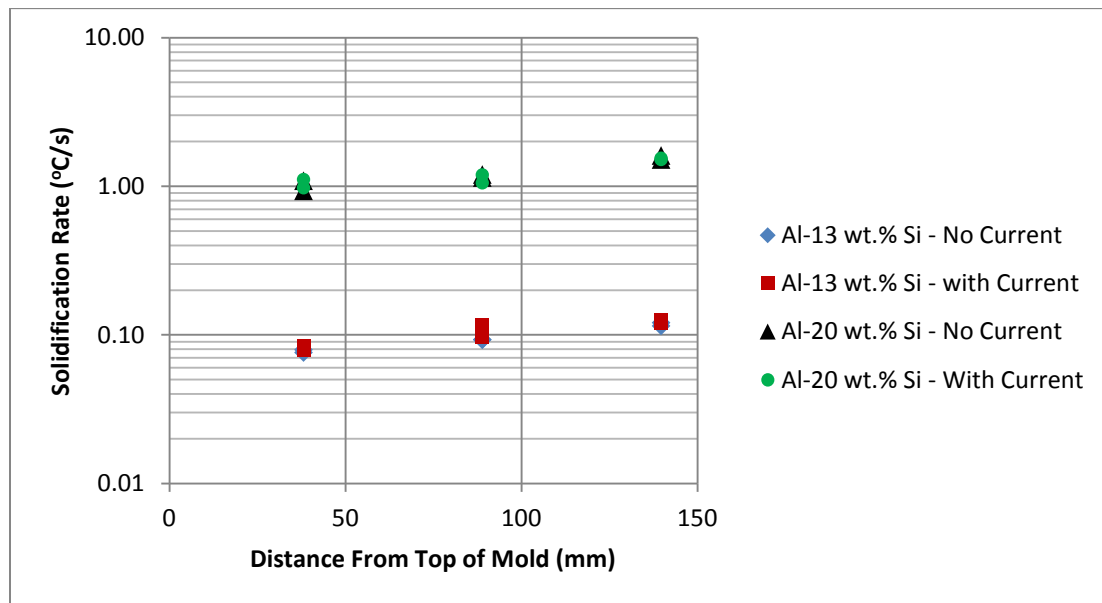


Figure 4.3: Solidification rates of each casting as a function of the distance from the top of the cast ingot.

4.4. Effects of Applied Electric Current on Cast Microstructure

The effect of the applied electric current on the cast microstructure of hypereutectic Al-Si alloys was investigated. The microstructural details of concern were primary silicon particles, eutectic silicon particles, and eutectic aluminum dendrite cells.

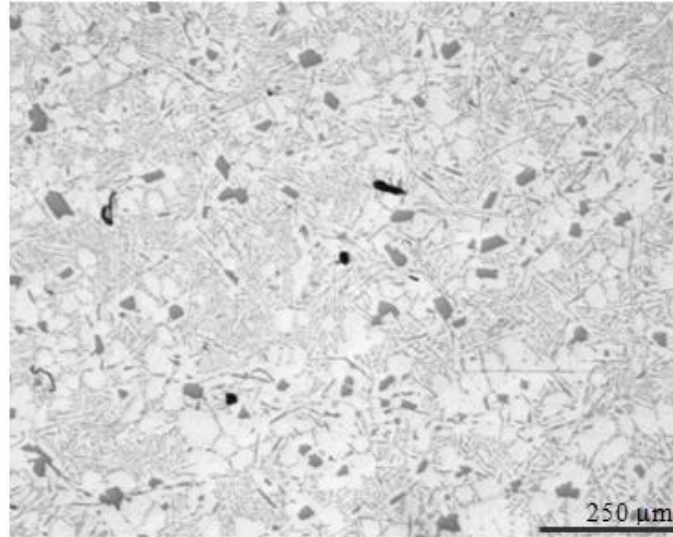


Figure 4.4: Optical photomicrograph at 100x magnification of representative Al-13 wt.% Si cast microstructure, showing primary silicon particles, eutectic silicon particles, and eutectic aluminum dendrite cells.

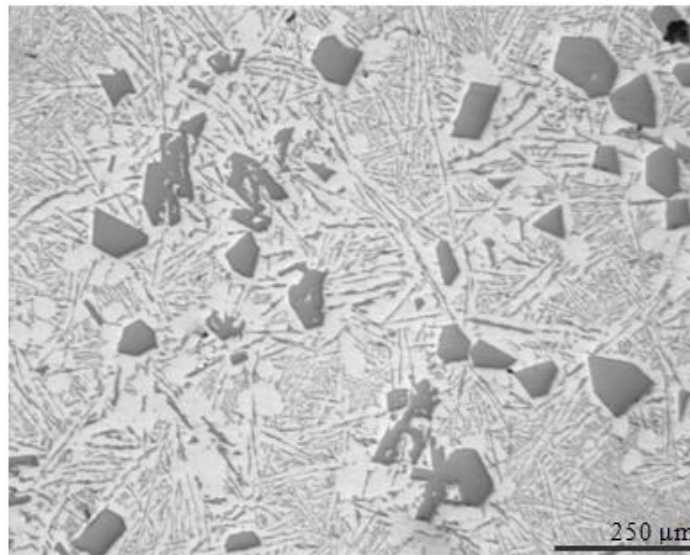


Figure 4.5: Optical photomicrograph at 100x magnification of representative Al-20 wt.% Si cast microstructure, showing eutectic silicon particles, eutectic aluminum dendrite cells, and a large volume fraction of primary silicon particles.

4.4.1. Dendrite Cell Size

The change in dendrite cell size as a function of the application of an electric current during solidification was quantitatively measured. This was performed manually for each sample at 200x magnification using the Leco IA32 image analysis software. Areas where dendrite cells were clearly visible were identified in each sample, and the widest part of each visible dendrite was measured, as shown in Figure 4.7. Thirty measurements were taken from each sample. Because two castings were made for each condition, this equates to sixty data points that were used for comparison for each casting location, for each composition. Statistical significance was not immediately found for the Al-20 wt.% Si castings, so an additional thirty data points were collected for each sample, equating to a total of 120 data points for each condition at this composition. A summary of results for each condition is shown in Table 4.2.

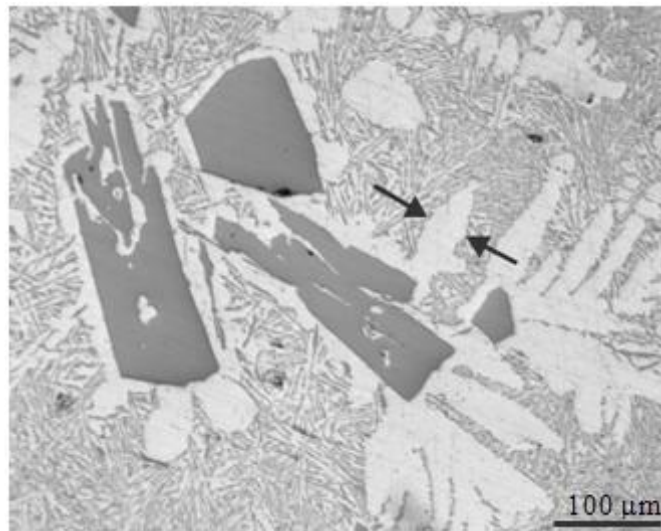


Figure 4.6: Optical photomicrograph at 200x magnification showing an example of how each dendrite cell was measured at its widest point at locations where dendrites were clearly visible.

The results in Table 4.2 show that for each location in the castings, the mean dendrite cell size was reduced by electric current in all cases, with the exception of the bottom location in the Al-20 wt.% Si composition.

Table 4.2: Average dendrite sizes and standard deviations for each composition and casting condition.

Composition	Condition	Distance From Top of Ingot (mm)	Avg (μm)	Std Dev (μm)
Al-13 wt.% Si	No Current	38.1	37.79	12.18
		88.9	34.75	12.37
		139.7	31.42	10.13
	With Current	38.1	34.86	10.39
		88.9	25.83	12.01
		139.7	23.09	8.69
Al-20 wt.% Si	No Current	38.1	38.01	11.74
		88.9	36.69	9.33
		139.7	26.10	9.79
	With Current	38.1	36.74	12.98
		88.9	32.88	13.01
		139.7	26.19	10.23

Table 4.3: Percent reduction in dendrite cell size resulting from the application of electric current during solidification with respect to distance from top of mold and composition.

Composition	Distance From Top of Ingot (mm)	% Reduction
Al-13 wt.% Si	38.1	7.8%
	88.9	25.7%
	139.7	26.5%
Al-20 wt.% Si	38.1	3.4%
	88.9	10.4%
	139.7	-0.3%

Dendrite cell size is strongly dependent on solidification rate, and no significant differences in solidification rates were observed between samples taken from similar locations for each alloy composition. This is shown graphically in Figure 4.3. Since the application of an electric current affected the dendrite cell size, but not solidification rate, dendrite cell size as a function of local solidification time and local solidification rate was investigated. Figure 4.7 shows average dendrite cell size with respect to local solidification time for each alloy composition with and without the electric current treatment. Figure 4.8 shows the average dendrite cell size with respect to local solidification rate for each alloy composition with and without the electric current treatment. These graphs show that the dendrite cell size, with respect to local solidification time and rate, does not drastically change with the application of an electric current during solidification.

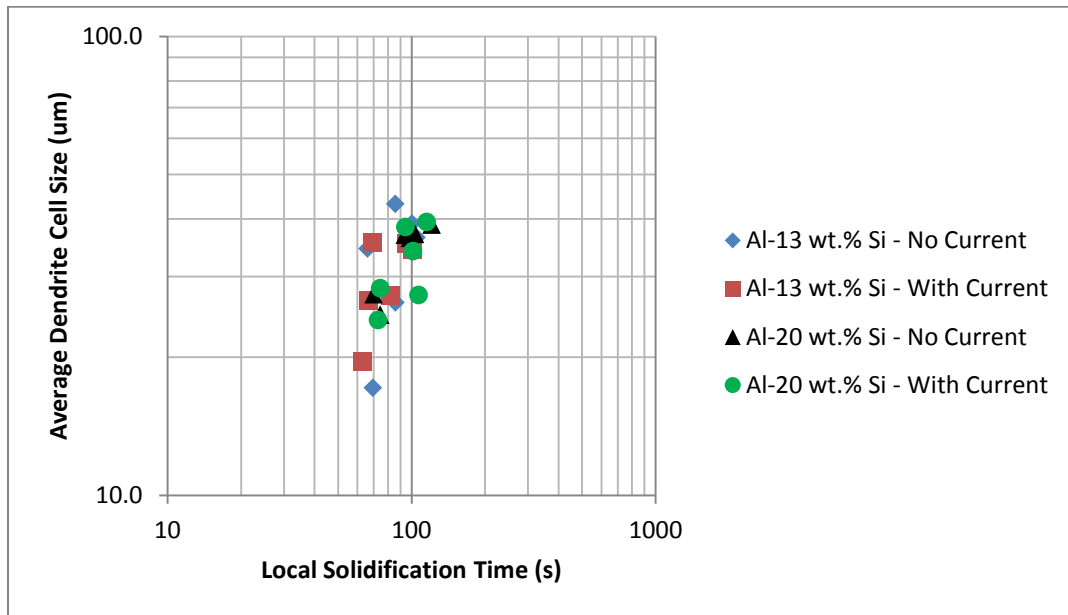


Figure 4.7: Average dendrite cell size as a function of alloy composition and application of electric current during solidification with respect to the local solidification time.

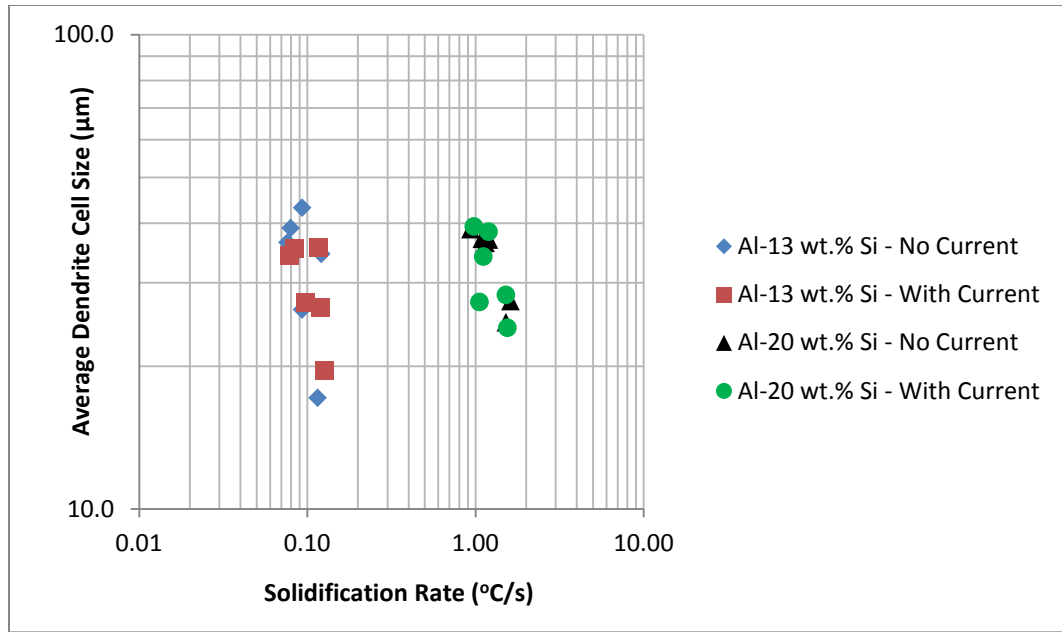


Figure 4.8: Average dendrite cell size as a function of alloy composition and application of electric current during solidification with respect to local solidification rate.

4.4.2. Primary Silicon Particles

Figure 4.9 shows representative photomicrographs which were selected from the samples taken from the center of the Al-20 wt.% Si castings. The size of the large primary silicon particles has not been dramatically decreased by the application of electric current during solidification. However, there appeared to be a new population of relatively smaller-size primary silicon particles in the castings solidified under the influence of an applied electric current. Figure 4.10 shows examples of the smallest primary silicon particles found in each condition. Clearly, the primary silicon particles in

the casting solidified under the influence of an electric potential are noticeably smaller in size. Figure 4.11 shows an example of these relatively smaller primary silicon particles.

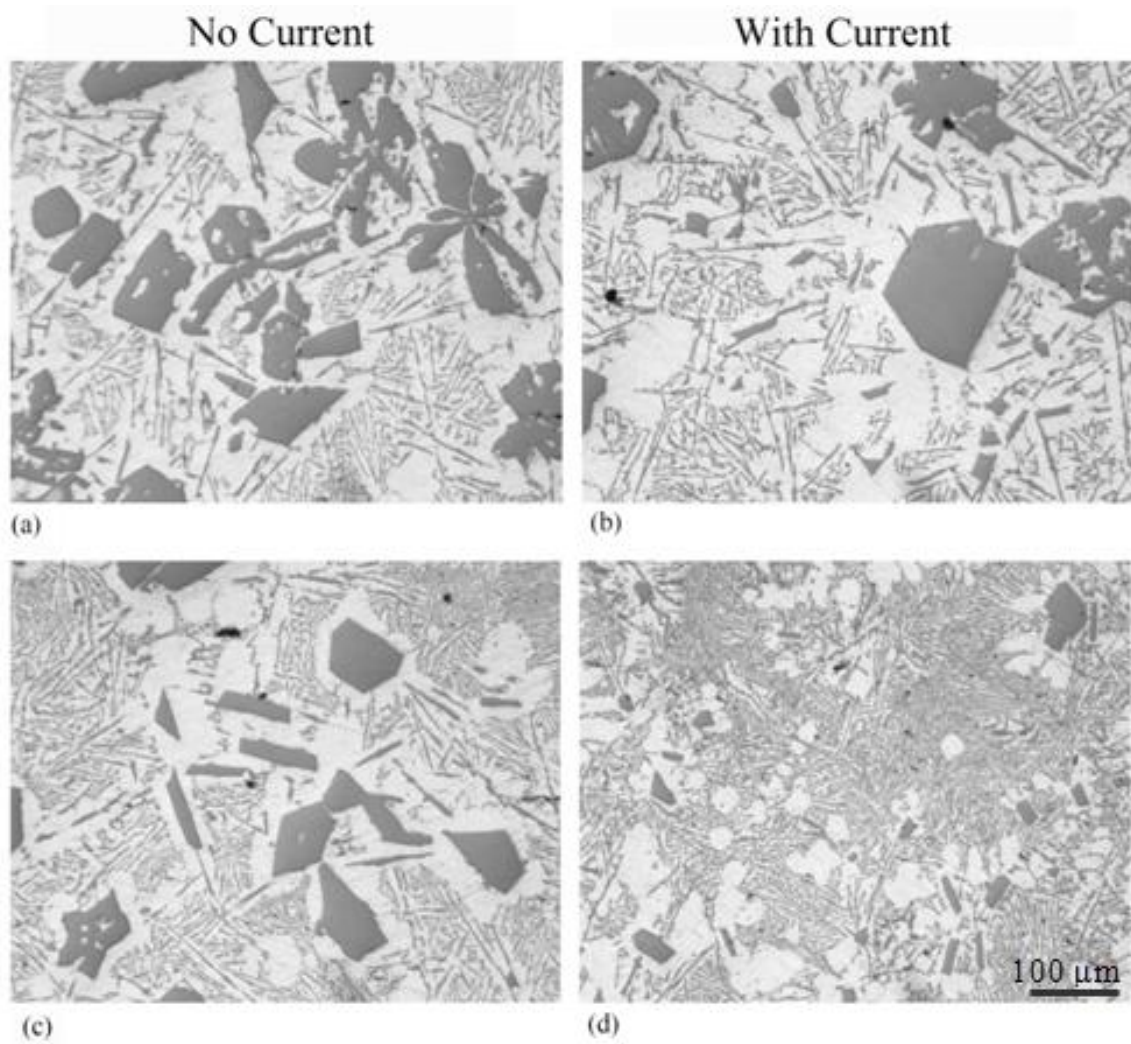


Figure 4.9: Optical photomicrographs at 200x magnification showing primary silicon particles in Al - 20wt.% Si without (a and c) and with (b and d) application of electric current during solidification.

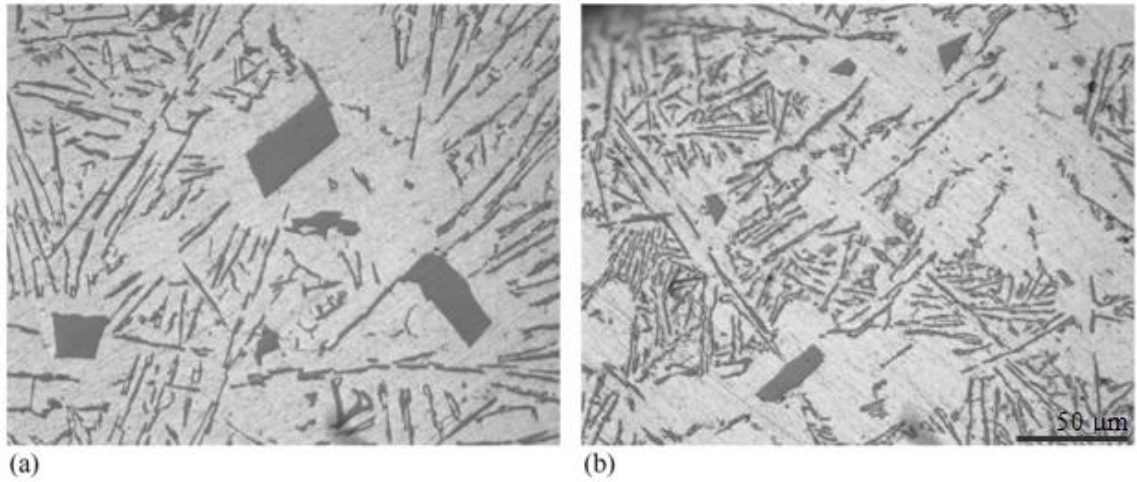


Figure 4.10: Optical photomicrographs at 500x showing the difference in size of the smallest primary silicon particles in samples from the centers of Al - 20wt.% Si castings solidified (a) without electric current and (b) with electric current.

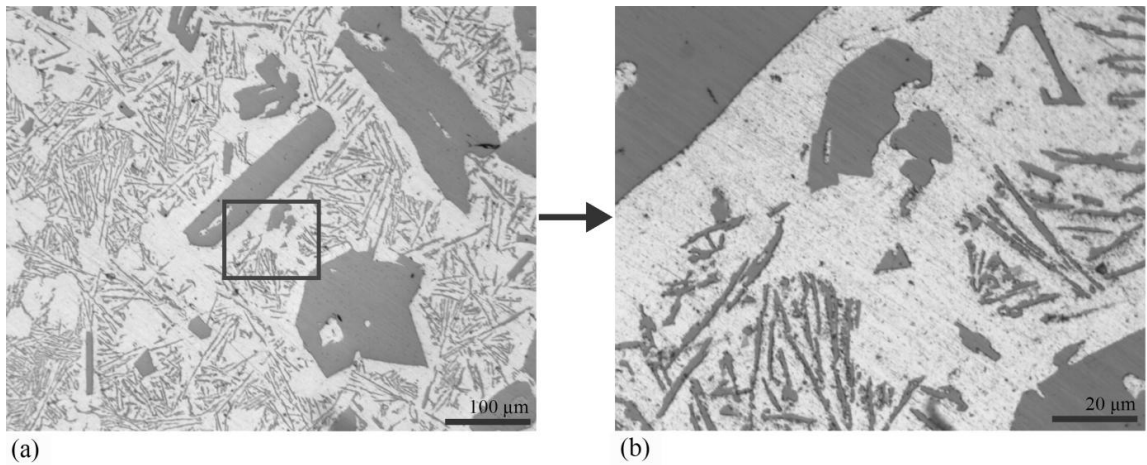


Figure 4.11: Very small primary silicon particles (200x magnification and 1000x magnification) in Al-20 wt.% Si with electric current applied during solidification.

Optical photomicrographs of primary silicon particles in the Al-13 wt.% Si alloys solidified with and without the application of an electric current are shown in Figure 4.12

and 4.13. Unlike in the Al-20 wt.% Si alloys, it does not appear that the application of electric current during solidification had an effect on the size or size distribution of the primary silicon particles in the Al-13 wt.% Si alloys.

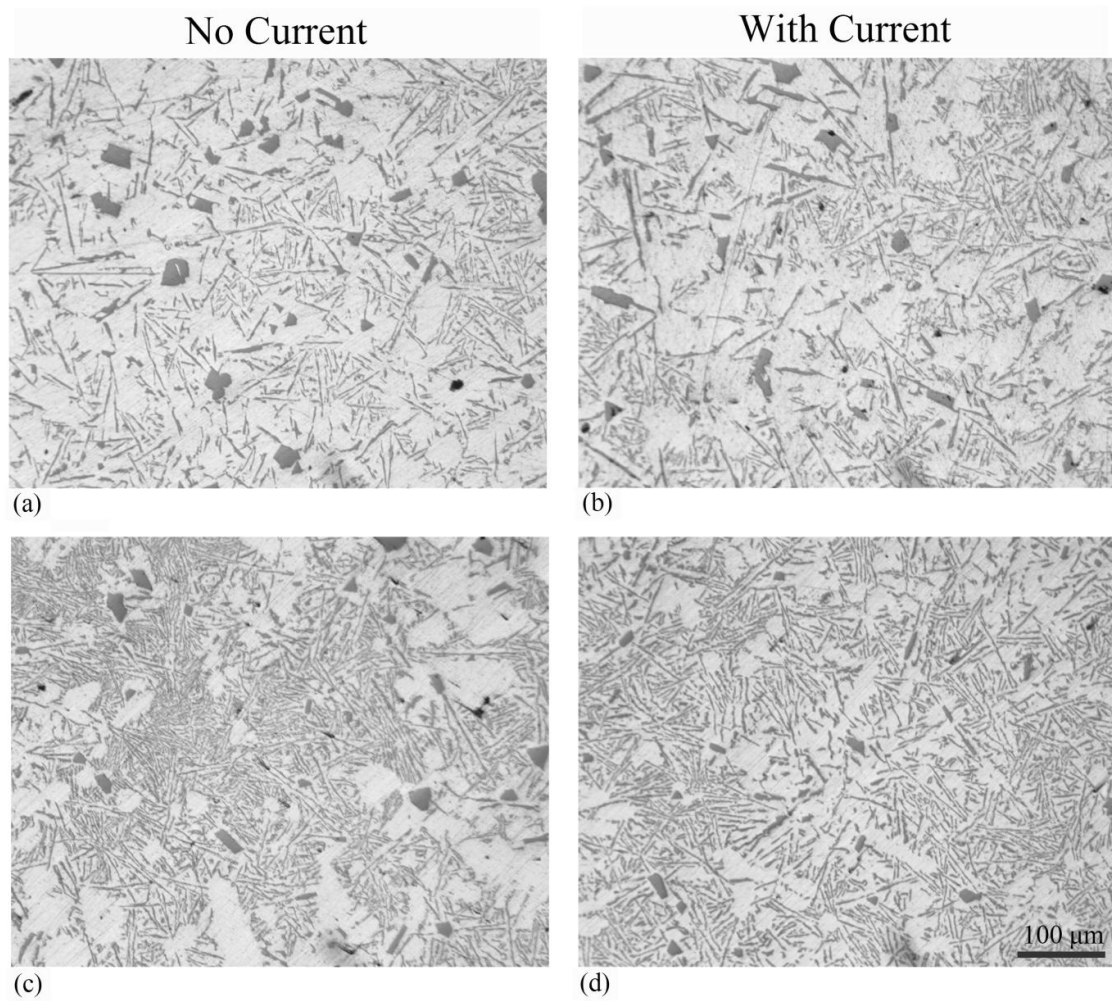


Figure 4.12: Optical photomicrographs at 200x magnification of primary silicon particles in Al-13 wt.% Si alloy without (a and c) and with (b and d) application of electric current during solidification.

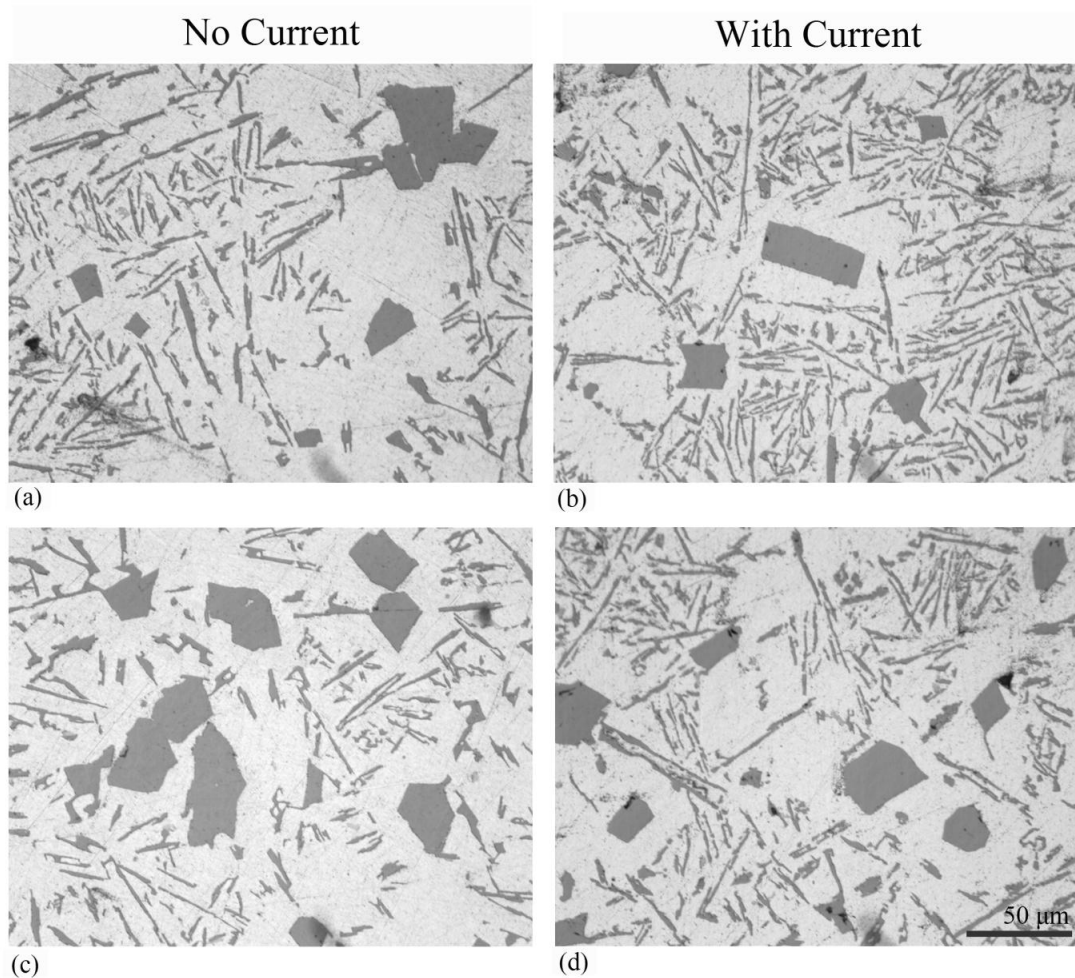


Figure 4.13: Optical photomicrographs at 500x magnification of primary silicon particles in Al-13 wt.% Si alloys cast without (a and c) and with (b and d) the application of electric current during solidification

4.4.3. Eutectic Silicon Particles

Figure 4.14 shows representative photomicrographs of the eutectic particles at 100x magnification for samples from the center of castings solidified with and without the electric current treatment. The eutectic silicon particles display a large size

distribution within a single sample, and these variations overlap for cases with and without the applied current. Qualitatively, there is no apparent effect on the size or size distribution of the eutectic silicon particles.

Figure 4.15 shows representative optical photomicrographs of the eutectic silicon particles at 500x magnification for samples solidified with and without the application of electric current. Again, a large variation in particle size is observed in both conditions, and it is also apparent that the morphology of the particles remains the same. In both conditions, the morphology of the eutectic silicon particles are needle or plate-like.

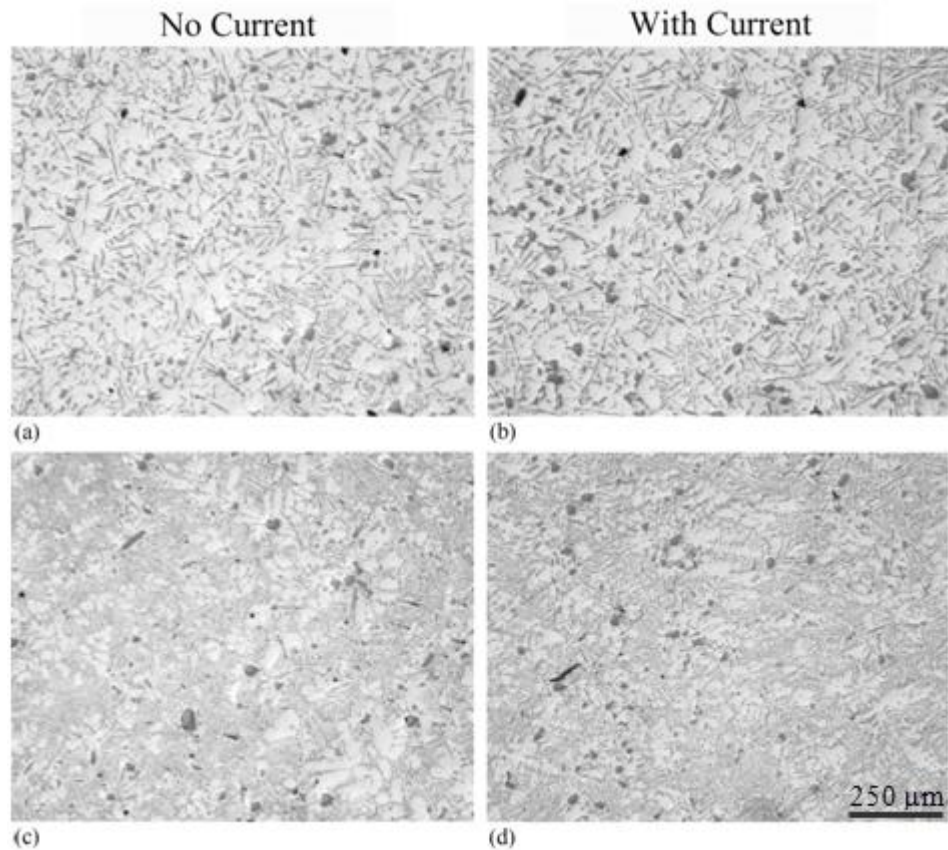


Figure 4.14: Optical photomicrographs at 100x magnification showing the large size distribution of eutectic silicon particles within a particular sample from Al - 13wt.% Si castings without current application (a and c) and with current application (b and d).

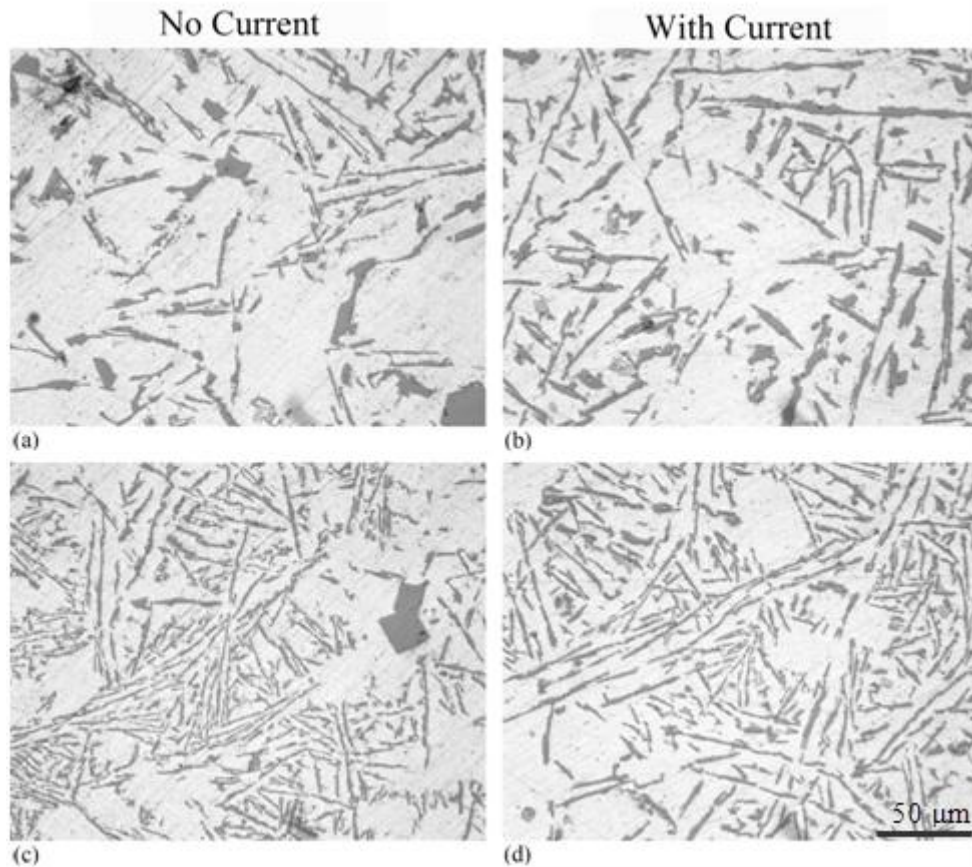


Figure 4.15: Optical photomicrographs at 500x showing no significant change in morphology of the eutectic silicon particles with the application of an electric current.

Photomicrographs shown are from samples at the center of the castings.

4.5. Discussion

The results obtained in this study have demonstrated the application of an electric current of approximately $500\text{mA}/\text{cm}^2$ during solidification has the following effects on the cast microstructure of hypereutectic Al-Si alloys:

- (i) The average dendrite cell size was reduced in all cases except the for the at the bottom of the Al-20 wt.% Si alloy.
- (ii) The applied electric current did not change the size of the largest primary silicon particles, but it appeared to have qualitatively increased the population of relatively smaller sized primary silicon particles in the Al-20 wt.% Si alloy.
- (iii) Qualitatively, the applied electric current did not change the size or size distribution of the primary silicon particles in the Al-13 wt.% Si alloy.
- (iii) The size, size distribution, and morphology of the eutectic silicon particles were not altered by the applied electric current during solidification.

4.5.1. Dendrite Cell Size

T-tests were used to determine the statistical significance of the reduction in dendrite cell size observed as a result of the application of electric current during solidification. Microsoft Excel was used to perform the t-tests, which were single tailed in nature and assumed unequal variances. Table 4.3 shows the percent reduction in dendrite cell size and p-values resulting from the t-tests performed on each set of measurements. All locations in the Al-13 wt.% Si compositions had decent statistical significance ($p < 0.1$), and the center of the Al-20 wt.% Si composition had very good

significance ($p = 0.005$), although the top and bottom samples from the Al-20 wt.% Si castings had very poor significance ($p > 0.2$).

Table 4.4: Percent reduction in dendrite cell size with application of electric current for each alloy composition as a function of distance from top of ingot and p-values resulting from t-tests comparing the corresponding data sets.

Composition	Distance From Top of Ingot (mm)	% Reduction	p-value
Al-13 wt.% Si	38.1	7.8%	0.079
	88.9	25.7%	0.055
	139.7	26.5%	0.078
Al-20 wt.% Si	38.1	3.4%	0.213
	88.9	10.4%	0.005
	139.7	-0.3%	0.473

The Al-13 wt.% Si castings in this study, in which the reduction of dendrite cell size as a function of the applied current was statistically significant for all regions of the castings, showed a reduction of 7.8% at the top, and 25.7% and 26.5% at the middle and bottom thermocouple locations, respectively. The 26% reduction in dendrite size agrees reasonably well with results reported by Anyalebechi and Tomaswick [1] for Al 7050 castings solidified under the influence of electric currents varying from 465 mA/cm² to 930 mA/cm², and applied in both steady and pulsed manners. The dendrite cell sizes were reduced by 29% and the reported effect was not dependent on electric current density or manner of current application. This also falls within the range of 25% to 40% reduction in size of graphite flakes reported by Vaschenko et al. for gray cast iron solidified in a sand mold [2].

Anyalebechi and Tomaswick [1] speculated that the reduction in dendrite cell size was caused by a shear stress induced fragmentation of dendrite arms. Peltier, Thompson, and Joule heating at the solid-liquid interface may have caused strong localized convection currents that produced enough force to shear off solidified dendrite arms. These solid fragments would then float into the melt and serve as additional nuclei. The electric current densities used in this study were similar to those used by Anyalebechi and Tomaswick, and they also found refinement of dendrite cell size with steadily applied electric current. Considering these similarities to this study, in both methods and results, it is likely that similar mechanisms were responsible. Therefore, dendrite shearing by localized convection currents may be the mechanism for the dendrite cell size refinement observed in this study.

Nakada et al. [3] and Jianming et al. [4] proposed similar dendrite arm fragmentation theories for refinement. However, they speculated that the mechanism for dendrite arm shearing was the pinch force caused by high density electric pulses. Barnak et al. [5] calculated that the pinch force caused by electric current densities of 1000-1500 A/cm² did not create shear stresses high enough to break dendrite arms in Pb-Sn alloys. Considering Barnak et al.'s [5] calculations, and because the electric current application in this study was several orders of magnitude lower than studies by Nakada et al. [3] and Jianming et al. [4] and was not pulsed, it is unlikely that the dendrite shearing caused by the pinch force was the mechanism for the observed refinement of dendrite cell size.

Anyalebechi and Tomaswick [1] also suggested that a secondary mechanism in which the applied electric current dramatically changed the solid-liquid interfacial energy, leading to an increase in nucleation rate. Qin and Zhou [6] theoretically studied

this refinement mechanism and calculated the level of refinement as a function of electric current density for a variety of pure metals. Their calculations did not predict significant refinement at electric current densities below 10^3 A/cm². However, they made no predictions for comparatively more complex multi-component systems. In the case of dendrite arms in hypereutectic Al-Si alloys, the interfacial energy of concern is between solid primary silicon particles and eutectic composition liquid transforming into eutectic aluminum dendrites. It is possible that this interfacial energy is affected to a greater extent by the application of electric current in pure metals as predicted by Qin and Zhou [6]. Alternatively, this mechanism may make a small contribution in combination with other mechanisms to result in the observed refinement of dendrite cell size.

For the Al-20 wt.% Si alloys, the change in the dendrite size was not statistically significant in the samples from the top and bottom of the castings. Good statistical significance ($p = 0.005$) was found at the center of the casting, but the reduction was modest in comparison to the Al-13 wt.% Si alloy at 10%. This result suggests that the presence of a large volume fraction of primary silicon particles in the melt at the time when the eutectic aluminum dendrites formed during the eutectic reaction changed the interaction between the electric current and the solidifying eutectic aluminum dendrite cells. This may have been a result of increased Joule and Peltier heating caused by the large volume fraction of primary silicon particles. At the eutectic temperature for the Al-Si binary system, pure silicon has an electrical resistivity approximately four orders of magnitude greater than that of aluminum [7-9]. Joule heating is directly proportional to resistance, and as such, for a given current density, local heating caused by the Joule effect may be increased by a larger volume fraction of primary silicon particles. Peltier

heating is a function of the interface between two dissimilar materials. As such, this heating would increase with the increased volume fraction of primary silicon particles. Additionally, the Peltier effect is closely related to the thermoelectric effect, which is in turn related to the Seebeck coefficient. The Seebeck coefficient for pure silicon is approximately two orders of magnitude greater than that for aluminum [9]. Therefore, it is possible that a greater quantity of primary silicon present during the eutectic reaction would have a dramatic effect on the amount of Peltier heating produced. These sources of heat may have decreased the local solidification rate, and increased the dendrite cell size.

4.5.2. Primary Silicon Particles

Of the previous studies on the effects of electric current on Al-Si alloys, only Hongsheng et al. [10] and Ban et al. [11] experimented on hypereutectic Al-Si alloys and assessed the effect of such a treatment on the primary silicon particles. Hongsheng et al. [10] found that the high density, pulsed electric current reduced the size of the primary silicon particles and made the particles more spherical in shape. These results agree with this study because a reduction in the size of some of the primary silicon particles was observed. However, the effect of the electric current pulses on the size distribution of the silicon particles was not discussed. Hongsheng et al. [10] theoretically showed that the application of electric current reduced the free energy barrier for nucleation for aluminum, but suppressed nucleation for silicon. This caused an increase in nucleation rate for primary silicon particles, resulting in smaller, more uniformly distributed

particles. This mechanism may be applicable to the apparent increase in relatively smaller sized primary silicon particles in this study. It is possible that the electric current partially suppressed the primary silicon nucleation. This may have produced some primary silicon particles that nucleated near the liquidus temperature and had sufficient time to grow, but suppressed further nucleation to lower temperatures, resulting in comparatively smaller sized primary silicon particles.

Ban et al. [11] also studied the application of high density electric pulses to hypereutectic Al-Si alloys during solidification. They concluded that the refinement was caused by the pinch force breaking solidified primary silicon particles into smaller pieces. This mechanism is not applicable to this study because the electric current application was not pulsed, and because the electric current density was several orders of magnitude smaller than that used by Ban et al. [11].

4.5.3. Eutectic Silicon Particles

The lack of an observed effect of the applied direct and steady electric current on the size and morphology of the eutectic silicon particles in this study is not consistent with the reported effects of pulsed electric current in the technical literature [10,12,13]. For example, Hongsheng et al. reported that the application of a high density pulsed electric current during solidification reduced the length of the eutectic silicon particles [10]. The electric current density used for this study was not reported, but the voltage used was 2000V, discharged via a capacitor bank. As such, it may be assumed that the

electric current density was much larger than that used for the present study. Xu et al. [12] experimented with both direct and alternating electric currents on hypoeutectic Al-Si alloys. They reported similar results as Hongsheng et al. [10], in that the length of the eutectic particles was decreased, and noted that the result was more dramatic with the alternating current. Again, the electric current density was not reported, but electric currents of 220A were used, so assuming that the cross sectional area of the casting was on the same order of magnitude as this study, the current density was much greater.

The electric current density used in this study was several orders of magnitude less than that used by Hongsheng et al. [10] and Xu et al. [12]. Additionally, electric current was administered in a steady rather than pulsed [10] or alternating [12] manner. Considering that no change in the eutectic silicon particles was observed in this study, it may be concluded that the effect of the application of electric current during solidification to Al-Si alloys on the eutectic particles is either a function of electric current density, or the manner of application. Hongsheng et al. [10] suggested that the mechanism of refinement was suppression of the nucleation of silicon. This effect is likely a function of current density, and thus may not have been significant in this study with a current density of 500 mA/cm². Xu et al. [12] attributed refinement of the eutectic silicon particles to vibration induced by the alternating current, similar to refinement via electromagnetic vibration. The current in this study was applied in a direct manner, so this effect was not applicable.

Zhang et al. [13] applied pulsed electric current densities ranging from 800 A/cm² to 2400 A/cm² to Al-Si alloys of eutectic composition. They reported that this procedure produced areas of fine lamellar structures of eutectic silicon, distributed among the usual,

randomly oriented needle or plate-like eutectic structure. Figure 4.16 shows an example of these structures. No similar structures were found in the samples prepared for this study. Zhang et al. [13] concluded that the fine lamellar eutectic silicon structure was formed because the Lorentz force generated by the pulsed electric current constantly fed solute to the solidifying region. However, the Lorentz force is only generated under a time dependent magnetic field [14]. Steady applied electric current, such as used in this study, is not time dependent, and therefore, does not generate the Lorentz force. Therefore, the lack of such fine lamellar structures in the samples from this study is not surprising.

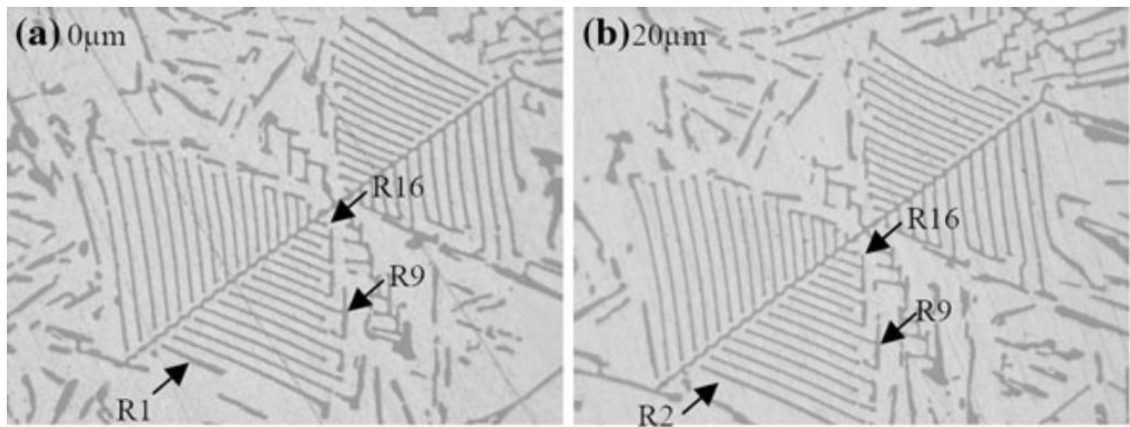


Figure 4.16: Lamellar eutectic Si structure induced by the application of high density pulsed electric current during solidification of eutectic Al-Si alloy [13].

4.6. References

- [1] P. N. Anyalebechi and K. M. Tomaswick, "Effect of Application of Electric Current During Solidification on the Cast Microstructure of Aluminum Alloy 7050," in *EPD Congress 2009*, 2009, pp. 541-554.

- [2] K. Vashchenko, D. Chernega, S. Vorob'ev, N. Lysenko, and Y. Yakovchuk, "Effect of Electric Current on the Solidification of Cast Iron," *Metallovedenie i Termicheskaya Obrabotka Metallov*, Mar. 1974, vol. 3, pp. 62-65.

- [3] M. Nakada, Y. Shiohara, and M. Flemings, "Modification of Solidification Structures by Pulse Electric Discharging," *ISIJ International*, 1990, vol. 30, no. 1, pp. 27-33.

- [4] L. Jianming, L. Shengli, and L. Hantong, "Modification of Solidification Structure by Pulse Electric Discharging," *Scripta metallurgica et materialia*, 1994, vol. 31, no. 12, pp. 1691-1694.

- [5] J. Barnak and A. Sprecher, "Colony (grain) size reduction in eutectic Pb-Sn castings by electroplusing," *Scripta metallurgica et materialia*, 1995, vol. 32, no. 6, pp. 879-884.

- [6] R. Qin and B. Zhou, "Effect of Electric Current Pulses on Grain Size in Castings," *International Journal of non-Equilibrium Processing*, 1998, vol. 11, pp. 77-86.
- [7] S. G. Teodorescu, R. A. Overfelt, and S. I. Bakhtiyarov, "An Inductive Technique for Electrical Conductivity Measurements on Molten Metals," *International Journal of Thermophysics*, 2001, vol. 22, no. 5, pp. 1521-1535.
- [8] G. Pearson and J. Bardeen, "Electrical Properties of Pure Silicon and Silicon Alloys Containing Boron and Phosphorus," *Physical Review*, 1949, vol. 75, no. 5, pp. 865-883.
- [9] W. Fulkerson, J. Moor, R. Williams, R. Graves, and D. McElroy, "Thermal Conductivity, Electrical Resistivity, and Seebeck Coefficient of Silicon from 100 to 1300 K," *Physical Review*, 1968, vol. 167, no. 3, pp. 765-782.
- [10] D. Hongsheng, Z. Yong, J. Sanyong, C. Ruirun, and Z. Zhilong, "Influences of pulse electric current treatment on solidification microstructures and mechanical properties of Al-Si piston alloys," *China Foundry*, 2008, vol. 6, no. 1, pp. 24-31.
- [11] C. Ban, Y. Han, Q. Ba, and J. Cui, "Influence of Pulse Electric Current on Solidification Structures of Al-Si Alloys," *Materials Science Forum*, 2007, vol. 546-549, pp. 723-728.

- [12] G. Xu, J. Zheng, Y. Liu, and J. Cui, "Effect of electric current on the cast microstructure of Al-Si alloy," *China Foundry*, 2005, vol. 2, no. 3, pp. 171-175.
- [13] Y. Zhang et al., "Influence of Electric-Current Pulse Treatment on the Formation of Regular Eutectic Morphology in an Al-Si Eutectic Alloy," *Metallurgical and Materials Transactions B*, Mar. 2011, vol. 42, no. 3, pp. 604-611.
- [14] H. K. Moffatt, "Electromagnetic Stirring," *Physics of Fluids A*, May 1991, vol. 3, pp. 1336-1343.

Chapter 5

Conclusions and Suggested Future Research

5.1. Conclusions

1. The application of 465-518 mA/cm² steady electric current to Al-13 wt.% Si alloy during solidification reduced the average dendrite cell size throughout the casting by 7.8%-26.5%, with statistical significance ($p < 0.1$). The application of electric current during solidification to the Al-20 wt.% Si alloy did not change the dendrite cell size at the top or bottom of the casting, but it reduced the average dendrite cell size at the center of the casting by 10.4% ($p = 0.005$).
2. For Al-20 wt.% Si alloy, the application of 465-518 mA/cm² steady electric current during solidification did not reduce the size of the largest primary silicon particles, but it appeared to have qualitatively increased the population of relatively smaller size primary silicon particles. The application of electric current during solidification did not appear to have any effect on the size or size distribution of primary silicon particles in the Al-13 wt.% Si alloy.
3. The application of a steady electric current during solidification did not appear to have any effect on the size or morphology of the eutectic silicon particles in both the Al-13 wt.% Si and Al-20 wt.% Si alloys.

5.2. Suggested Future Research

In this study, no quantitative measurement with an image analyzer of the size, size distribution, or morphology of the primary and eutectic silicon particles in either the Al-13 wt.% Si or Al-20 wt.% Si alloys was performed, primarily due to time constraints. Future work should involve quantitative characterization of the Si particles that form during solidification of the hypereutectic Al-Si alloys with an image analyzer software package. In particular, the size and size distribution of the primary silicon particles in the Al-20 wt.% Si alloy should be measured as a function of the applied electric current during solidification and location within each casting.

The electric current in this study was supplied in a steady manner and with relatively small current density. It would be of interest to investigate the effect of a steadily applied current during solidification on the microstructure of hypereutectic Al-Si alloys at higher current densities. Also, studying these effects at various solidification rates might reveal details about the mechanism of refinement. Varying solidification rates could be accomplished using different mold materials or by chilling the mold during the casting procedure.

Numerous other studies investigating the effect of an applied electric current during solidification on the microstructure of various materials involved the use of different current application methods. One application method of particular interest is using an AC current, rather than a DC current. It would be of interest to investigate the effect on the microstructure of such a current applied during solidification to hypereutectic Al-Si alloys, and to compare these results to those found using DC

application at similar current densities. This experimentation would be simple to implement using the same equipment used for this study, as the power supply involved was also capable of AC current application. It would also be of interest to investigate the effects of different levels of pulsed electric current density applied during solidification on the cast microstructure of hypereutectic Al-Si alloys.

Additionally, a theoretical study of the proposed mechanisms for the electric current-induced refinement in hypereutectic Al-Si alloys is of interest. This will include the evaluation of the interfacial energy between solid primary silicon particles and liquid Al-Si as a function of the applied current density. This interfacial energy could then be used to evaluate the effect of the electric current on the free energy barrier for nucleation. Also, a more thorough investigation of the magnitude of Joule and Peltier heating as a function of current density is of interest. A quantitative analysis of these effects might explain why significant dendrite cell size reduction was observed uniformly in the Al-13 wt.% Si alloy, but not in the Al-20 wt.% Si alloy.